INVESTIGATION OF ELECTRICAL AND OPTICAL PROPERTIES OF BULK III-V TERNARY SEMICONDUCTORS

THESIS

Travis C. Gomez, Captain, USAF

AFIT/GMS/ENP/09-M01

DEPARTMENT OF THE AIR FORCE
AIR UNIVERSITY

AIR FORCE INSTITUTE OF TECHNOLOGY

Wright-Patterson Air Force Base, Ohio

AFIT/GMS/ENP/09-M01

INVESTIGATION OF ELECTRICAL AND OPTICAL PROPERTIES OF BULK III-V
TERNARY SEMICONDUCTORS

THESIS

Presented to the Faculty

Department of Engineering Physics

Graduate School of Engineering and Management

Air Force Institute of Technology

Air University

Air Education and Training Command

In Partial Fulfillment of the Requirements for the

Degree of Master of Science in Material Science
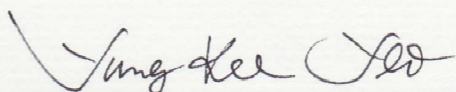
Travis C. Gomez, BS

Captain, USAF

March 2009

INVESTIGATION OF ELECTRICAL AND OPTICAL PROPERTIES OF BULK III-V TERNARY SEMICONDUCTORS

Travis C. Gomez, BS
Captain, USAF

Approved:

_____
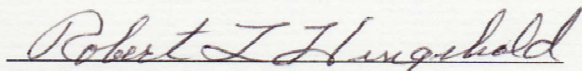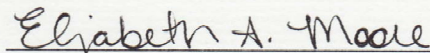Dr. Yung Kee Yeo (Chairman)

11 March 2009
_____
Date

_____
Dr. Robert L. Hengehold (Member)

11 Mar 2009
_____
Date

_____
Dr. Elizabeth A. Moore (Member)

11 March 2009
_____
Date

Abstract

Bulk grown III-V ternary semiconductors of $In_{0.08}Ga_{0.92}Sb$ and $In_{0.15}Ga_{0.85}As$ were investigated through Hall-effect and photoluminescence measurements to determine carrier concentration, mobility, sheet resistivity, and luminescence spectrum. In the past, epitaxial layers of ternary compounds have been grown on binary compound substrates, and thus very limited lattice matched ternary alloys were available. Recently, bulk grown ternary substrates have been developed, and it has presented a renewed interest in using these substrates to grow high quality ternary compounds for use in many next generation optoelectronic devices. The results of photoluminescence (PL) study for the $In_{0.15}Ga_{0.85}Sb$ sample show the exciton bound to neutral acceptor (A^o,X) transition peak at 675 meV along with a donor-shallow acceptor pair transition peak at 650 meV, and the donor-deep acceptor pair transition peak at 628 meV. The Hall-effect measurements show that this sample is an n-type material with carrier concentration of about $4x10^{17}/cm^3$ and mobility of about 300 cm^2/Vs at room temperature. The $In_{0.80}Ga_{0.20}As$ sample is also an n-type material with a carrier concentration of $1.34x10^{16}/cm^3$ and a mobility of 9,670 cm^2/Vs at room temperature. The PL result of this sample shows a broad band to band peak at 572 meV. The PL taken at different positions of the sample show different band to band peak positions for the $In_{0.80}Ga_{0.20}As$ sample, indicating a slight inhomogeneity in Ga concentration, while the PL observed from the $In_{0.15}Ga_{0.85}Sb$ sample shows position independent. Although the current bulk grown ternary alloy materials may not be as great yet as we hope for a direct use in next generation optoelectronic devices, it will provide suitable substrates for which to grow epitaxial layers.

Acknowledgments

I would like to thank my advisor, Dr. Yung Kee Yeo, for his guidance throughout my research. A special thanks to Dr. Elizabeth Moore and Mr. Mike Ranft. You will never know how much you helped both in and out of the labs. Your patience with me will never be forgotten. Thank you to Lt Col Matthew Bohn and Mr. Greg Smith for your troubleshooting expertise. You saved my research. I would like to also thank Mr. Bill Trop and Mr. Rick Patton for ensuring I was always supplied with everything I needed to keep my research going. I would like to thank Dr. Shekar Guha of the Air Force Research Laboratory and Dr. Partha Dutta and Dr. Geeta Rajagopalan from United Semiconductor, L.L.C. for supplying me with samples with which I could conduct my research and also for providing valuable transmission measurements.

I would like to thank my two little angels for entertaining Mommy when I couldn't make it home on time. Thank you bringing me lunch when you knew I needed to see you. To my wife, you have once again put aside your life so that I could pursue another goal. Thank you for putting up with me while being the most amazing mother to our little ones. I could never have done this without your love and support.

Travis C. Gomez

Table of Contents

List of Figures

List of Tables

INVESTIGATION OF ELECTRICAL AND OPTICAL PROPERTIES OF BULK III-V TERNARY SEMICONDUCTORS

I. Introduction

Background

Epitaxial layers of ternary compounds have historically been grown on lattice mismatched binary compound substrates. This lattice mismatch limited the ability to extend the range of the mole fraction to higher values which, in turn, limited the ability to create compounds with specific band gap energies. With regards to this study, the indium mole fraction of $In_xGa_{1-x}Sb$ and $In_xGa_{1-x}As$ has been limited to the low end of the mole fraction range. The biaxial strain caused by lattice mismatching results in changes in the compounds band gaps, conduction band effective masses, and the valence band structure. [1] The thickness of epilayer growth on lattice mismatched substrates depends entirely on the percent of mismatch. As an approximation, a misfit of 1% can only yield an epilayer thickness of a few hundred angstroms. [1] In the case of $In_xGa_{1-x}As$, the lattice constant can change as much as 7.2% as the indium mole fraction increases from 0 to x=1. [2-4] The effects of lattice mismatching can be severe and may have such a large effect on the compound that it is rendered useless. Fig. 1 shows a schematic representation of strained layer epitaxy while Fig. 2 shows an example of misfit locations caused by such strain in $In_{0.3}Ga_{0.7}As$ grown on GaAs. Recently, bulk grown ternary substrates have been developed which has presented a renewed interest in using these substrates to grow high quality ternary compounds for use in many next generation optoelectronic devices. In the case of $In_xGa_{1-x}Sb$, the band gap ranges from 726 to 170 meV as the indium mole

1
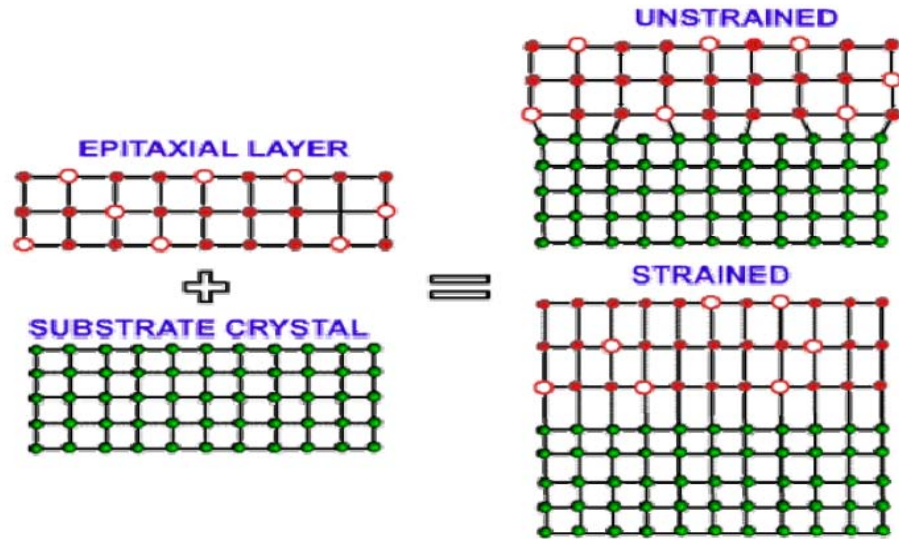
Figure 1. Schematic representation illustrating the negative effects of a strained lattice caused from epitaxial layers grown on a lattice mismatched substrate. [5]
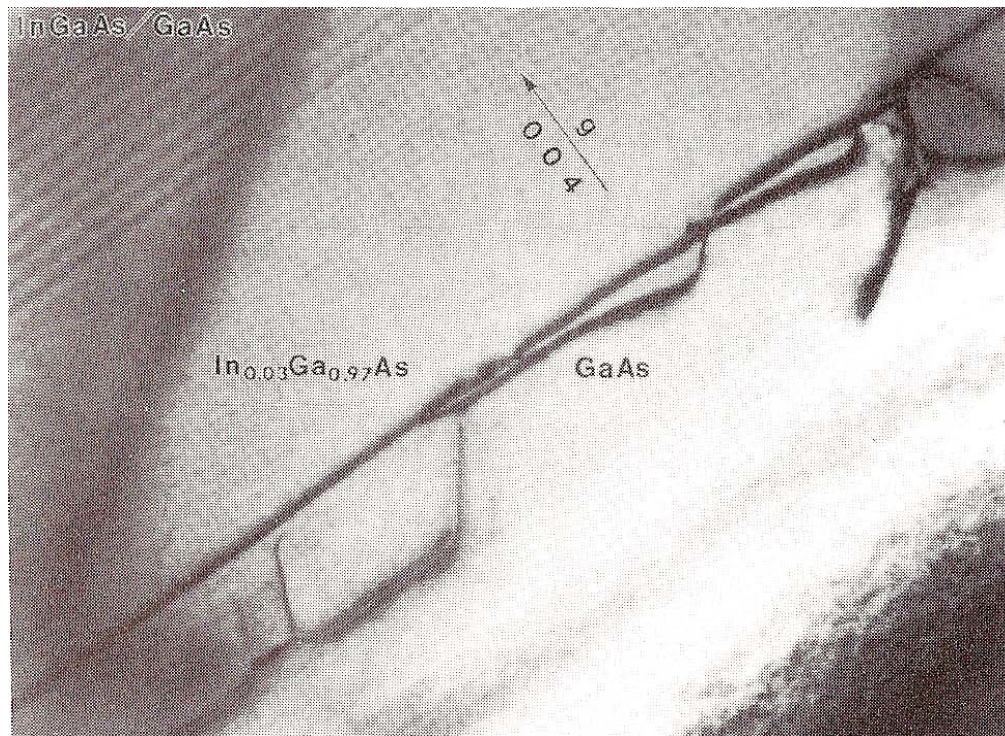
Figure 2. Cross-section transmission electron micrograph (TEM) showing an interfacial dislocation network caused by strain from a lattice mismatch in molecular beam epitaxial growth of $In_{0.3}Ga_{0.7}As$ on GaAs (f=2%). [1]

fraction varies from 0 to 1. Therefore, devices utilizing this material could operate in the mid infrared (IR). The band gap range for $In_xGa_{1-x}As$ is 1,424 to 360 meV as the indium mole fraction varies from 0 to 1, also making it a candidate for IR devices. [1] Their high electron mobility, typically around 33,000 cm^2/Vs at room temperature, will enable them to take high frequency and high speed devices to the next level. [6] The wavelengths in which these devices operate make them ideal candidates as lasers for optical fiber communication. Such lasers have not been constructed due to the fact that the lattice mismatch between the ternary material with the desired indium mole fraction and the substrate prevents the minimum thickness from being attained. [7] Many devices, such as optical amplifiers, superluminescent diodes, optoelectronic integrated circuits, IR diodes and detectors, field effect transistors, and microwave devices, would benefit from the ability to produce improved crystal quality material, grown either as bulk or epilayers, with a thickness that can be used in a production environment. [6-22] Providing quality bulk material in which to grow epilayers of theoretically unlimited thickness will enable these materials to be produced quicker and at a much lower cost. In addition, it may be possible that these bulk grown substrates are of high enough quality that they can be directly utilized for such applications. For instance, bulk material is actually desired for tunable lasers, semiconductor optical amplifiers, and superluminescent diodes which require very flat and wide gain spectrums. [8] In either case, whether using the bulk material for direct applications or as a substrate for growing previously unattainable thicknesses of epilayer material, these bulk ternary semiconductors will lead the way in the next generation of devices.

Research Objectives

Photoluminescence data as a function of temperature, laser intensity, and sample position will be used to investigate residual impurities and defects in bulk grown $In_xGa_{1-x}Sb$ and

In$_x$Ga$_{1-x}$As alloys, as well as exploring the compositional homogeneity. The samples used in this study were grown via the multi-component zone melting growth method. By studying the luminescence spectra, the band structure of each material will be revealed, to include the energy band gap and any other recombination transitions that may occur. In addition, characterization of various electrical properties as a function of temperature will be investigated through Hall effect measurements. The conductivity, carrier concentration, and mobility obtained from Hall effect measurements are key parameters in which all semiconductor materials are measured. The quality and performance of a semiconductor material is evaluated with these parameters.

Limitations

The samples used for photoluminescence measurements had energy band gaps of 680 and 572 meV which is in the wavelength range where there is a high probability of being affected by atmospheric absorption. It can be seen from the atmospheric absorption spectrum, shown in Fig. 3, that water and carbon dioxide block absorption in the 1.7 to 2.0 μm range. To account for this, the photon path from the sample chamber window through the spectrometer was purged with nitrogen gas. These extra precautions to seal the photon path allowed for the assumption that the entire photon path was free from atmospheric effects.
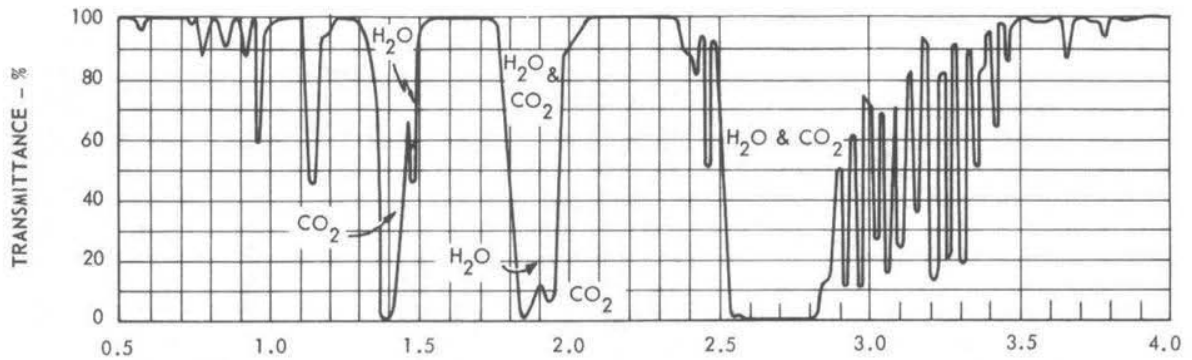
Figure 3. Atmospheric absorption from 0.5 to 4.0 μm for infrared wavelengths (wavelength units are in μm).

[23]

4

The measurement of the laser power was not precise. The sensor's power reading fluctuates approximately 50 mW, and does not settle on an exact number. In order to minimize this error, the sensor was placed in front of the laser path and allowed to settle for one minute before approximating the laser power. This provided a consistent method to measure the power.

II. Literature Review

Relevant Research

Electrical Characterization

There has been a significant amount of research conducted on $In_xGa_{1-x}Sb$ epilayer grown material. Wooley and Gillett conducted research on the electrical properties of $In_xGa_{1-x}Sb$ solid ingots prepared by slow freezing techniques of various indium compositions. Their research found the indium rich samples had a smooth variation of each parameter that was studied. In their study, they found the conductivity of $In_{0.24}Ga_{0.76}Sb$ varied from 100 ohm^{-1}cm^{-1} at 670 K to 5 ohm^{-1}cm^{-1} at 300 K. As temperature dipped below 300 K, the conductivity rose slightly before beginning to decrease again at 180 K. By the time it reached liquid nitrogen temperatures it was back down to approximately 5 ohm^{-1}cm^{-1}. [24] Magno *et al*. studied epilayer $In_{0.27}Ga_{0.73}Sb$ grown by molecular beam epitaxy and found the n-type samples to have carrier concentration of 9×10^{16} cm^{-3} and mobility of 11×10^3 cm^2/V-s at room temperature. [25] Gao *et al*. studied single crystals with high indium mole fractions of 0.77 grown by a new growth technique, melt epitaxy, and found a high electron mobility of 8.05×10^4 cm^2/V-s and low carrier density of 1.70×10^{15} cm^{-3} at 77 K. They also found the conductivity of the material at 77 K was 21.9 ohm^{-1}cm^{-1}. They concluded that these values are indicative of high purity material. [17] It will be useful to compare these values with the values obtained for the $In_{0.15}Ga_{0.85}Sb$ bulk grown samples used in this study to determine the crystalline quality of the material.

Like $In_xGa_{1-x}Sb$, epilayer grown $In_xGa_{1-x}As$ has also been researched in the past. Goldberg and Schmidt found the electron mobility at 300 K to be 12×10^3 cm^2/V-s for epilayer $In_{0.47}Ga_{0.53}As$. They also determined the electron mobility for $In_xGa_{1-x}As$ at 300 K can be predicted with the following equation [26],

$$(40 - 80.7(x-1) + 49.2(x-1)^2) \bullet 10^3 \frac{cm^2}{Vs} \qquad (2.1)$$

Lideikis *et al*. found the electron mobility of p-type $In_{0.53}Ga_{0.47}As$ to be approximately 2,100 cm^2/V-s, an increase of 400 cm^2/V-s over similarly grown material with an indium mole fraction of 0.16. [10] Thobel *et al*. also found that electron mobility increases with an increase in indium mole fraction from about 0.82×10^4 cm^2/V-s at x=0 to approximately 1.1×10^4 cm^2/V-s at x=0.5. [27] Their desire to have $In_xGa_{1-x}As$ with higher indium mole fractions was limited by the epilayer thickness that can be obtained due to the lattice mismatch with the GaAs substrate. Oliver *et al*. found the electron mobility at 300 K for an $In_{0.47}Ga_{0.53}As$ sample was 1.38×10^4 cm^2/V-s which had a carrier concentration of 2×10^{15} cm^{-3}. [14] They also took measurements at liquid nitrogen temperature and found the electron mobility increased to 7.00×10^4 cm^2/V-s, as did the carrier concentration to 3.5×10^{14} cm^{-3}. [14]

Optical Characterization

Optical characterization has also been accomplished on epilayer grown $In_xGa_{1-x}Sb$. Vankova *et al.* conducted photoluminescence measurements on metalorganic vapour phase epitaxial grown (MOVPE) $In_xGa_{1-x}Sb$ with indium mole fractions less than 0.06. [28] They observed that GaSb and $In_xGa_{1-x}Sb$ had similar temperature and laser power dependence with respect to the highest energy transitions. The same similarities were observed between the bound exciton recombination at 801 meV in GaSb and $In_xGa_{1-x}Sb$'s lower energy line. [28] Their work identifies excitons bound to native acceptors, recombination of a free electron at the native acceptor, donor bound excitons, the band-to-band transition, as well as other acceptor related transitions that occur in the photoluminescence spectra of GaSb, $In_{0.01}Ga_{0.99}Sb$, $In_{0.015}Ga_{0.985}Sb$, $In_{0.02}Ga_{0.98}Sb$, $In_{0.025}Ga_{0.975}Sb$, and $In_{0.035}Ga_{0.965}Sb$. Glaser *et al.* conducted low temperature photoluminescence on $In_{0.27}Ga_{0.73}Sb$ in order to determine the crystalline quality and

7

band gap energy. They reported a peak energy of 560 meV at 1.6 K. [20] Matsuura *et al*. used electrical property studies to determine band diagram characteristics for p-type $In_{0.2}Ga_{0.8}Sb$. They identified two acceptor levels at $E_v + 25$ meV and $E_v + 86$ meV, where E_v is the valence band maximum. [29] Bignazzi *et al*. discovered a longitudinal optical (LO) phonon replica for the 777 meV donor-acceptor pair peak located 33 meV away at 744 meV. [19]

Optical characterization research has also been conducted on epilayer grown $In_xGa_{1-x}As$, as well as InAs epilayers. Fang *et al*. conducted work on InAs epilayers. They observed a band to band emission located at 415 meV at 10 K. [30] They also determined the difference between the bound exciton and electron-hole recombination peaks was approximately 3 meV. [30] Mirin *et al*. studied high quality $In_{0.3}Ga_{0.7}As$ quantum dots grown by molecular beam epitaxy on GaAs and found them to have room temperature band-to-band peak at 950 meV with a FWHM of only 28 meV. [7] The FWHM narrows to a value of 26 meV at 230 K before increasing until saturation to 33 meV at 140 K. [7]

In addition to the research work already noted, transmission measurements were previously taken on the samples used in this study. Dr. Shekhar Guha and his team at the Air Force Research Laboratory at Wright-Patterson Air Force Base, determined the band gap energy for the $In_{0.15}Ga_{0.85}Sb$ sample to be approximately 670 meV. They also determined the band gap energy of the $In_{0.80}Ga_{0.20}As$ to be approximately 680 meV.

Summary

Research on bulk grown III-V ternary semiconductor materials has not yet matured. Most of the research no $In_xGa_{1-x}Sb$ and $In_xGa_{1-x}As$ ternary materials has focused on epilayer grown material. However, similar trends in conductivity, mobility, carrier concentration, and radiative recombinations observed in epilayer material should also be found in bulk grown

material. This will aid in determining the consistency of the data as well as the crystalline

quality of the bulk material.

III. Experiments

Theory on Electrical Measurements

Hall effect measurements are used as a convenient method to determine the mobility and carrier concentration of semiconductor materials. These properties, along with the resistivity, will determine how well the semiconductor material will perform when used as an electronic device. Fig. 4 illustrates the sample geometry for measuring the Hall Voltage where V_H is the Hall voltage, v_H, where **B** is the applied magnetic field, **I** is the applied current, and v_d is the drift velocity. The samples used in this study were of arbitrary shape, the Van der Pauw method was used to conduct the Hall measurements. The Van der Pauw method does not require a square samples as depicted in Fig. 4. However, the indium contacts must be placed on the periphery of the sample in order to minimize edge effects. The Hall measurement system used in this study also required the samples to have a thickness of no more than 15 times the shortest length of any side and be simply connected. When a magnetic field is applied perpendicular to the sample
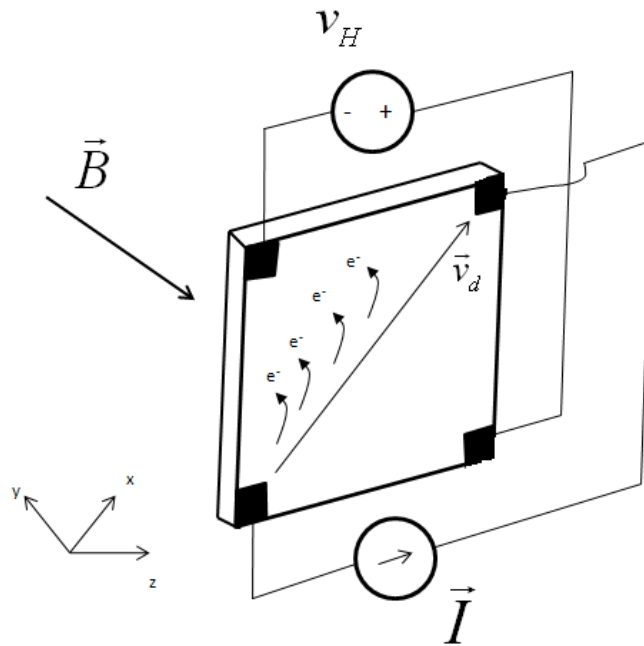
Figure 4. Geometry in which Hall effect measurements are taken.

surface and current is passed through the sample, the electrons are subjected to the Lorentz force. This causes the electrons to build up on one side of the sample which creates a voltage drop across the sample. The value of this potential difference can be calculated from the Lorentz force given by equation 3.1 [31]

$$\vec{F} = q\vec{E} + q(\vec{v} \times \vec{B}),$$ (3.1)

where q is the charge, **E** is the electric field, **v** is the charged particle velocity, and **B** is the magnetic field. When the electrons reach an equilibrium state, there is no force acting in the y-direction and this equation can be reduced to

$$F_y = qE_y - qv_xB_z = 0.$$ (3.2)

Rewriting this equation to include the current density, $J_x = nqv_x$, yields

$$E_y = \frac{J_xB_z}{nq},$$ (3.3)

where n is the carrier concentration. After multiplying both sides of equation 3.3 by the sample thickness, the more familiar Hall voltage is given to be

$$V_H = \frac{I_xB_z}{n_sq},$$ (3.4)

where n_s is the sheet carrier concentration. Once the Hall voltage is measured, the sheet carrier concentration can easily be calculated using equation 3.4. The conductivity of the material is given by the ratio of

$$\sigma_e = \frac{\vec{J}}{E} = n_sq\mu.$$ (3.5)

By inverting the material's measured resistivity, the ratio of current density to electric field is known. Since the sheet carrier concentration is already known, equation 3.5 can be solved for the Hall mobility.

Experimental Setup for Electrical Characterization

Hall effect measurements were taken using a Lake Shore Hall Effect Measurement system, diagramed in Fig. 5. Hall measurements were taken on one sample of $In_xGa_{1-x}Sb$ and one of $In_xGa_{1-x}As$ with indium mole fractions of 0.15 and 0.80, respectively. The samples were of arbitrary shapes with minimum length of approximately 10 mm and width of approximately 12 mm. Each sample had a thickness of 0.6 mm. The $In_{0.80}Ga_{0.20}As$ sample had measurements taken only at room temperature and 77 K, while the $In_{0.15}Ga_{0.85}Sb$ sample had measurements taken throughout the range of 10 to 300 K. In each case, the magnetic field was varied between -5 kG and 5 kG. The current for the $In_{0.80}Ga_{0.20}As$ sample was set at 100 mA for each temperature. The current setting for the entire temperature range of the $In_{0.15}Ga_{0.85}Sb$ was 1 mA. The samples were prepared by placing small indium contacts at the edge of each sample. Ohmic contacts are required in order to ensure accurate calculations of Hall effect measurements. Fig. 6 shows an example of contact placement on the $In_{0.15}Ga_{0.85}Sb$ sample. Contact locations were placed at the edge of the sample while ensuring there was material present across the entire straight line path between all contact points in order to prevent defects, cracks, and voids from distorting the data. A similar strategy was employed when applying indium contacts to the $In_{0.80}Ga_{0.20}As$ sample.
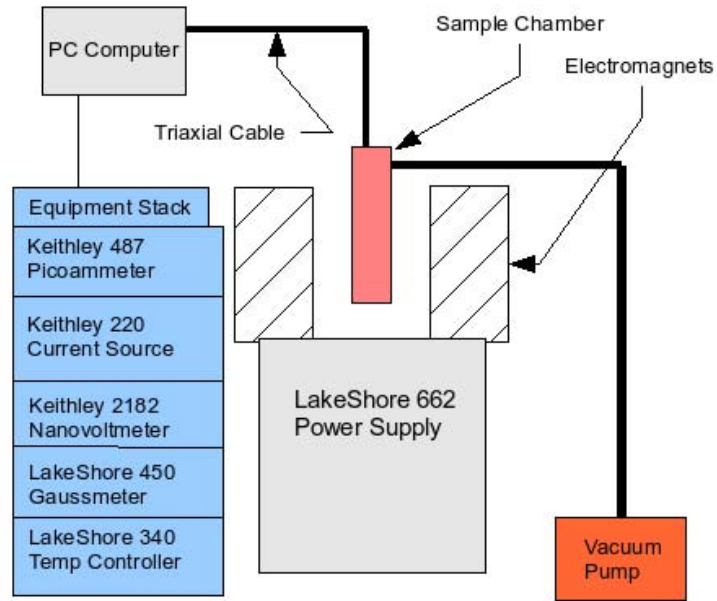
Figure 5. A diagram of the Lake Shore Hall Effect Measurement system. [32]
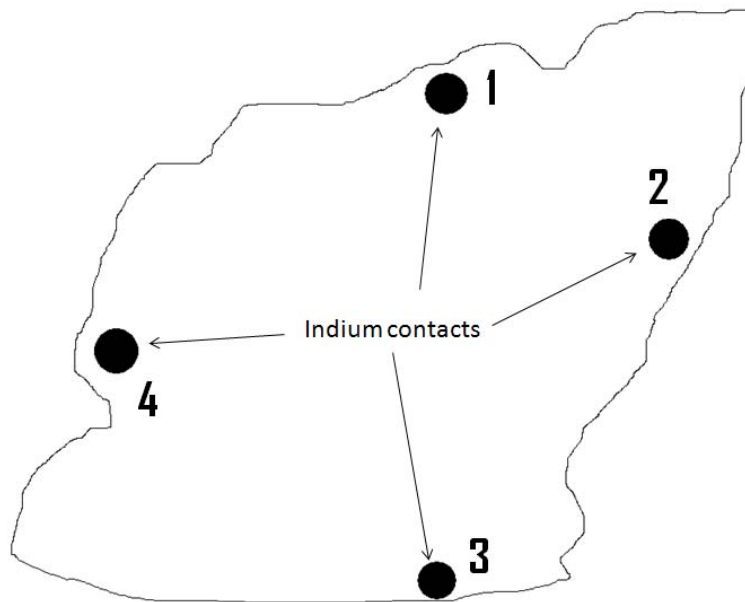
Figure 6. Indium contact locations of the In$_{0.15}$Ga$_{0.85}$Sb sample.

Theory on Optical Measurements

Photoluminescence measurements are used to determine the luminescence spectrum of a given material. Luminescence refers to a material's ability to absorb energy and then emit the energy at various wavelengths, which can be equal to the material's band gap energy as well as wavelengths attributed to other transitions discussed later in this section. Photoluminescence initiates this sequence by striking the material with photons using a laser beam. The photons are absorbed by the material and cause electrons in the valence band to move up into the conduction band through absorption. This creates an electron-hole pair. When the process reverses, the electron-hole pair releases its excess energy during the recombination process and in doing so it emits energy in both radiative and nonradiative recombination. The nonradiative energy is released as phonons and scatters as heat. The radiative energy is released as photons. When photoluminescence measurements are taken, the wavelengths of the emitted photons are observed and can be converted to energy values using

$$\varepsilon_g = \hbar\omega \tag{3.6}$$

where $\hbar$ is the reduced Planck's constant, 1.055 x 10^{-34} Joules-seconds and ω is the angular frequency. In terms of wavelength, this equation becomes

$$E_g = \frac{2\pi\hbar c}{\lambda} \tag{3.7}$$

where c is the speed of light, 2.998 x 10^8 m/s, and λ is the wavelength. This process is depicted in Fig. 7. Observing the transition peaks from the photoluminescence spectra gives insight into the band structure of the material. Common radiative transitions that take place in semiconductors are depicted in Fig. 8.
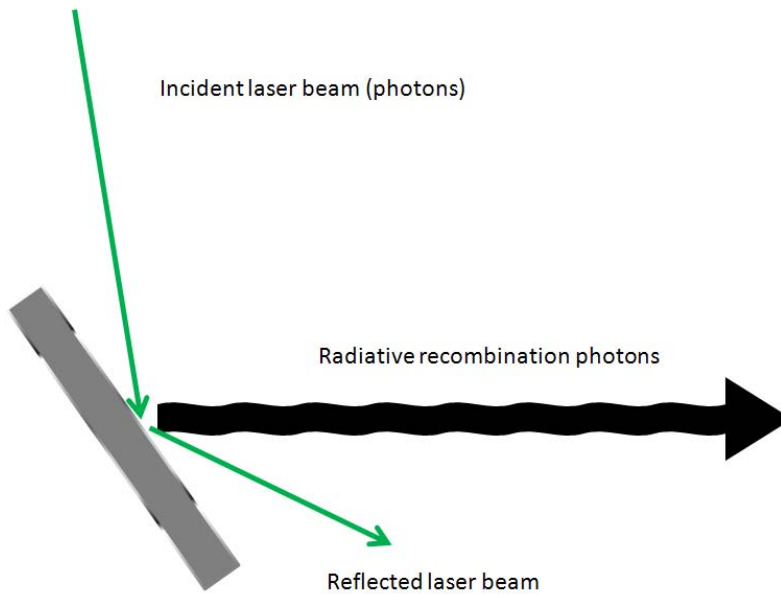
Figure 7. Illustration of the absorption of photons supplied by laser beam and emission of radiated photons by a semiconductor material.
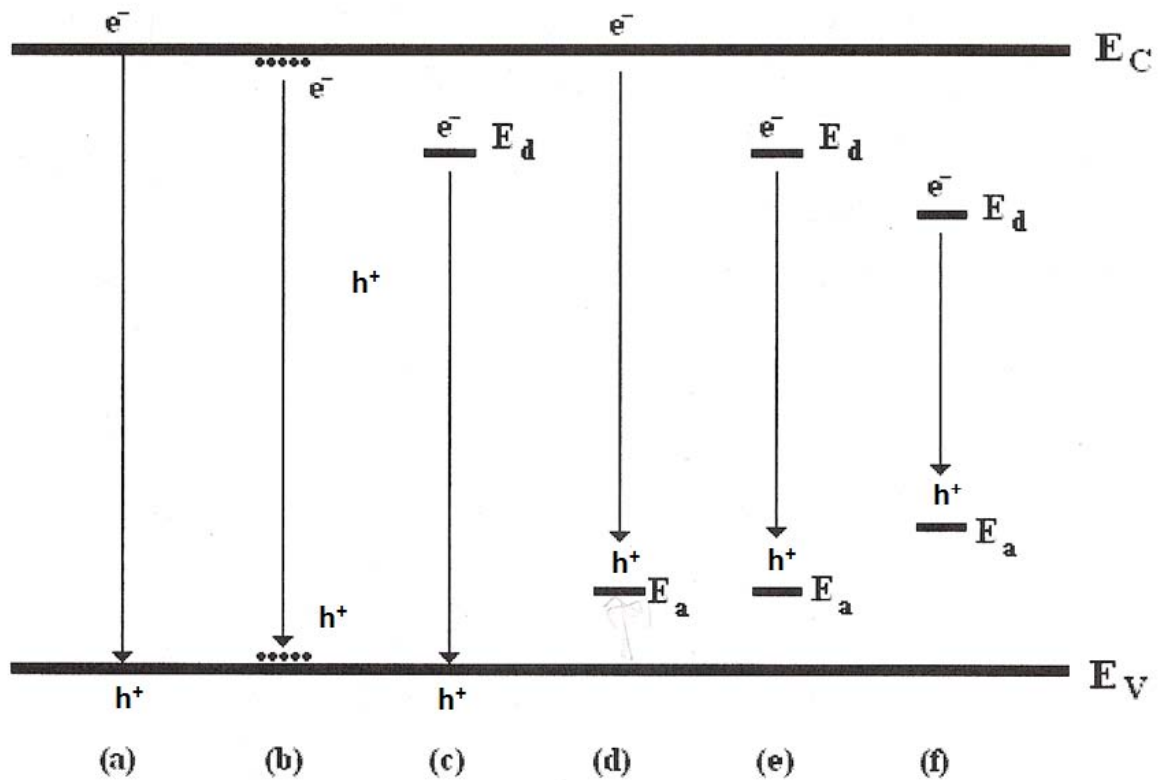
Figure 8. A two dimensional illustration of common radiative transitions that take place in semiconductors. Transitions shown are the band-to-band transition (a), free exciton transition (b), the neutral donor free hole recombination (c), a free electron transitioning to a neutral shallow acceptor (d), the donor acceptor transitions for shallow states (e), and the donor acceptor transitions for deep states. [33]

Experimental Setup for Optical Characterization

The optical properties of the material were investigated with photoluminescence measurements. A diagram of the experiment is shown in Fig. 9. It should be noted that while the preamplifier and 12V power supply for bias voltage were wired into the setup, the power supply was not operating correctly during the $In_{0.15}Ga_{0.85}Sb$ testing and as a result the voltage source was not turned on. However, the power supply problem was corrected before beginning the testing on the $In_{0.80}Ga_{0.20}As$ sample. The laser was a BeamLok Argon Ion laser emitting at 514.5 nm. The monocrometer was a SPEX 750M spectrometer with opening and exiting slits set at 3 mm and a grating with 600 grooves/mm blazed at 1.7 µm. Each scan was taken in 0.5 nm increments in wavelength with a dwell time of 0.5 s for the $In_{0.15}Ga_{0.85}Sb$ sample. The $In_{0.80}Ga_{0.20}As$ sample had the same dwell time, but the scanning rate was lowered to 0.2 nm increments in wavelength. The time constant on the lock-in amplifier was set to 300 ms during all scans. The optical chopper frequency was approximately 163.5 Hz. For laser power dependent photoluminescence measurements, the samples were subjected to multiple laser powers ranging from 100 to 750 mW at a fixed sample temperature. For the temperature dependent photoluminescence measurements, the sample temperatures were varied from 10 to 75 K. The measurements were also repeated at various locations on the sample to investigate the homogeneity of the material, as illustrated in Fig. 10.

1) Laser
2) Neutral Density Filter
3) Optical Chopper
4) Periscope
5) Iris
6) Laser Power Sensor
7) Sample Chamber
8) 100 mm CaF_2 Optical Lens
9) 300 mm CaF_2 Optical Lens
10) SPEX 750M Spectrometer
11) InSb Detector
12) Transimpedence Preamplifier
13) 12 V power supply
14) Lock-in Amplifier
15) Optical Chopper Frequency Control
16) DM303M Voltage Input Module
17) dM3000 SPEX Spectrometer Software CPU
18) SPEX MSD2 Spectrometer Controller
19) CPU

518 nm Laser Line
Emitted Photon Path

Figure 9. Experimental setup for photoluminescence measurements.

(i)   (ii)
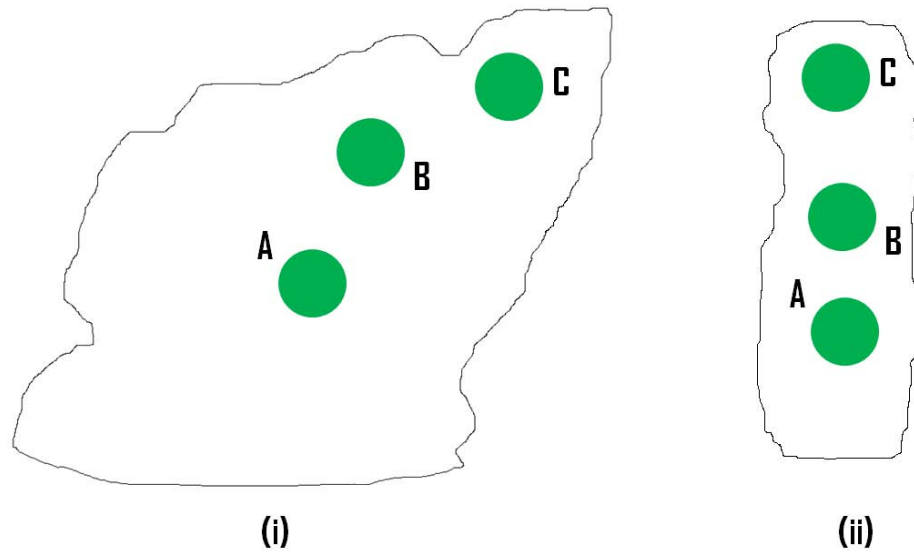
Figure 10. Locations on the (i) $In_{0.15}Ga_{0.85}Sb$ and (ii) $In_{0.80}Ga_{0.20}As$ samples where photoluminescence data was obtained.

17

IV. Results and Analyses

Results of Electrical Characterization Data

The $In_{0.15}Ga_{0.85}Sb$ sample provided useful information about the resistivity, mobility, and conductivity type. The results of Hall-effect/sheet-resistivity measurement data for this sample cannot be interpreted straight forwardly, not like other ordinary simple conductivity semiconductors. Therefore, the interpretation of these data is tentative at best. Probably, this sample may have some unique characteristics as shown in the results of Hall measurements presented here. When the ohmicity of the contacts was checked either from current-voltage (I-V) curve or curve tracer, it showed decent ohmic behavior. Fig.11 shows the resistivity data obtained in this study. Fig. 12 shows a conductivity plot as a function of temperature on a semi-log scale, and the conductivity plot of Wooley and Gillett's study on $In_xGa_{1-x}Sb$ is also shown in Fig. 13. [24] Our data seems to show two different mechanisms of conductivities. Equation 4.1 shows conductivity's dependence on carrier concentrations and mobilities in a semiconductor.

$$\sigma = q(n\mu_e + p\mu_h) \qquad\qquad (4.1)$$

where q is the electron charge, n is the electron concentration, μ_e is the electron mobility, p is the hole concentration, and μ_h is the hole mobility. [1] In Fig. 12, the higher temperature region with temperatures greater than 160 K is dominated by typical thermally ionized free carriers from impurities, which is why the conductivity increases rapidly with temperature. The conductivity of the center section, from approximately 160 K to 70 K, is decreasing. This is probably where the mobility becomes dominant over the carriers. Within this region, the mobility is decreasing due to lattice scattering. Below approximately 70 K, the conductivity remains about the same, which is probably due to impurity band conduction. Wooley and Gillett's study on $In_{0.24}Ga_{0.76}Sb$ solid ingots provided conductivity results that seem comparable to the $In_{0.15}Ga_{0.85}Sb$ from this

0   50   100   150   200   250   300

0.20

0.15

$In_{0.15}Ga_{0.85}Sb$
Current: 100 mA

Resistivity (ohm-cm)

0.10

0.05

0.00
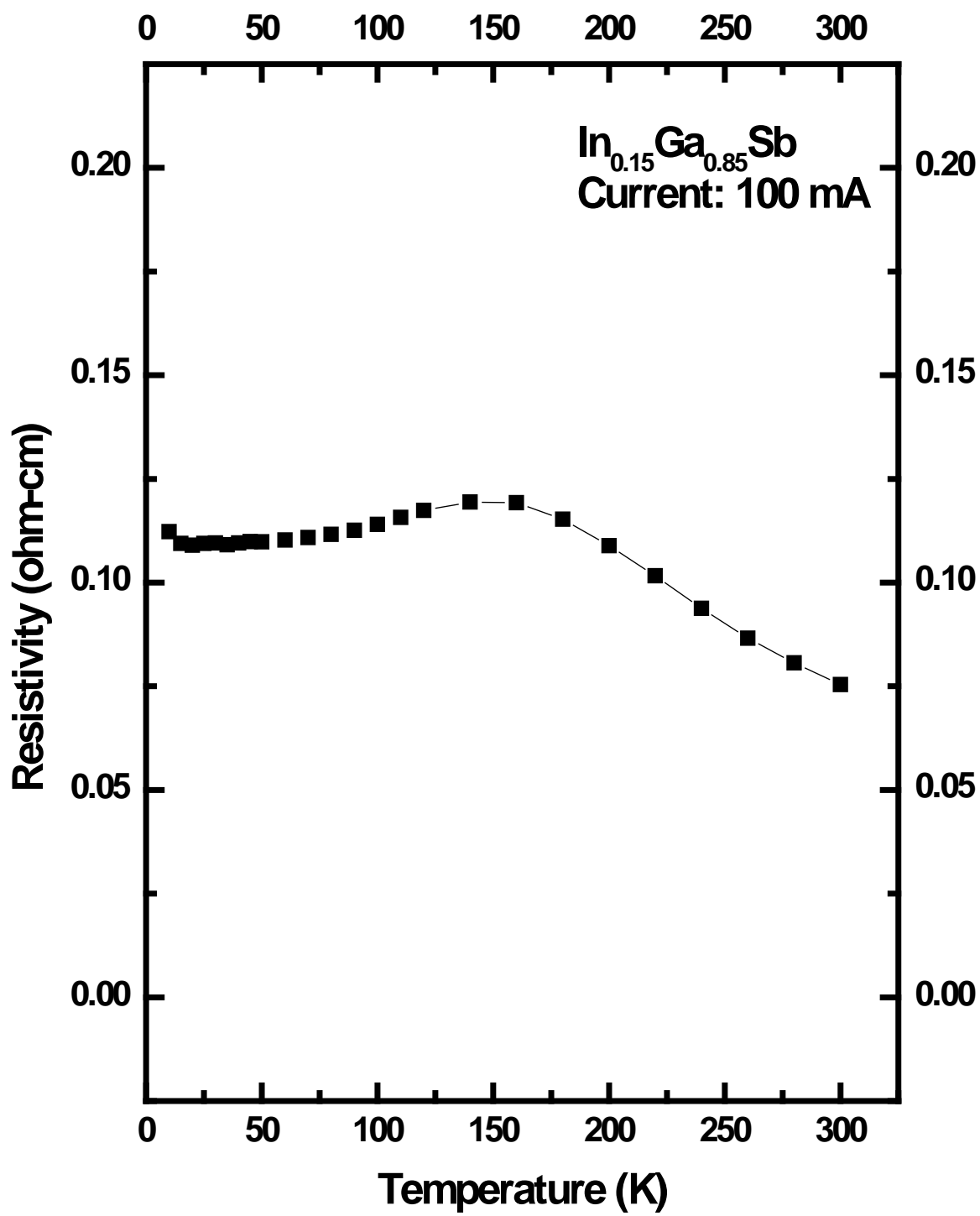
Temperature (K)

Figure 11. Resistivity as a function of temperature for $In_{0.15}Ga_{0.85}Sb$ measured with 100 mA of current.
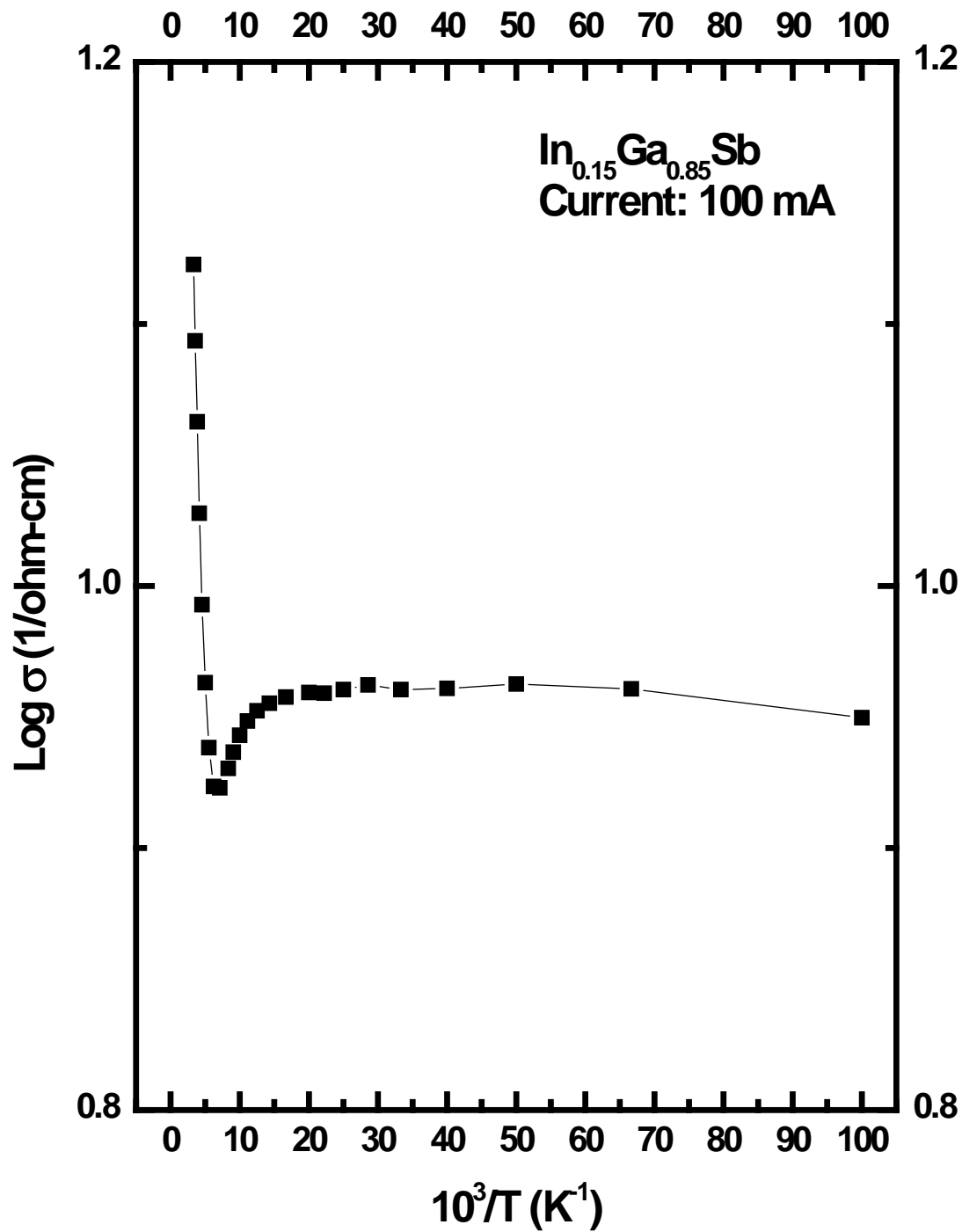
Figure 12. Conductivity as a function of inverse temperature for In$_{0.15}$Ga$_{0.85}$Sb measured with 100 mA of current.
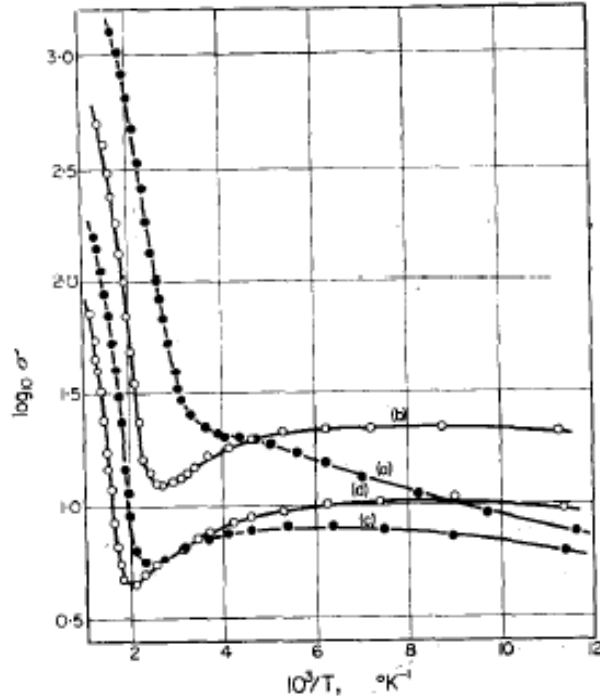
Figure 13. Conductivy as a function of inverse temperature taken from Woolley and Gillet's study on (a) $In_{0.90}Ga_{0.10}Sb$, (b) $In_{0.53}Ga_{0.47}Sb$, (c) $In_{0.24}Ga_{0.76}Sb$, and (d) $In_{0.06}Ga_{0.94}Sb$. [24]

study. However, the conductivity mechanisms of the two samples are very different. Their

results are due to typical intrinsic carrier conduction at low and high temperature regions,

respectively. With regards to mobility, studies on InSb and GaSb shown in figures 14 and 15,

respectively, show that the mobility tends to increase as the temperature rises from 10 to 30 K

due to impurity screening and then decrease as temperatures rise above 30 K due to lattice

scattering. [34-35] The mobility data obtained on the $In_{0.15}Ga_{0.85}Sb$ sample shown in Fig. 16

shows very different behavior than the mobility data shown in figures 14 and 15. The mobility

values are nearly constant below about 70 K, decreasing as temperature increases up to 160 K,

and then start to increase again as temperature increases. It should be noted that the mobility

values obtained in this study are much lower than the expected value of about 16,000 cm^2/Vs at

room temperature for n-type $In_{0.15}Ga_{0.85}Sb$. Goa *et al*. noted that high purity material yielded

21

higher mobility levels. [17] It is believe that this sample is fairly doped and showing impurity

band conduction. The effective mass within this narrow impurity band is much larger than in the

adjacent carrier band, and therefore, the mobility value is very low at lower temperatures up to

70 K for present
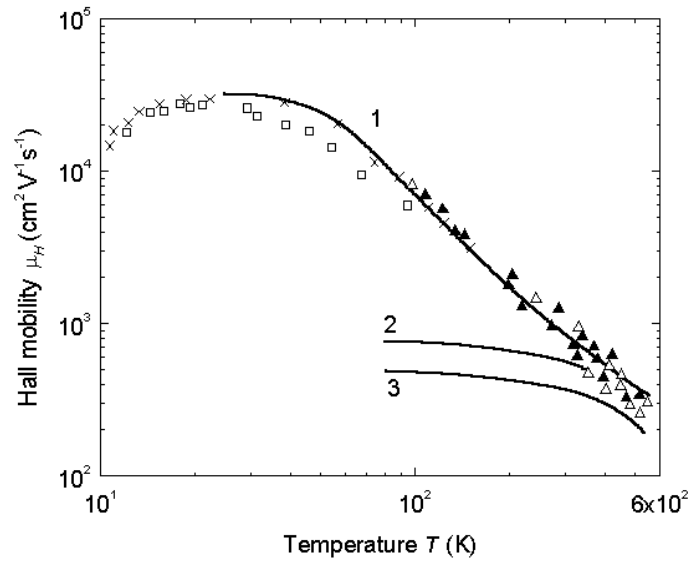
Figure 14. Hall mobility as a function of temperature for p-type InSb with (1) p_0=8x10^{14}, (2) p_0=3.15x10^{18}, and (3) p_0=2.5x10^{19}. [34]

Figure 15. Hall mobility as a function of temperature data for several GaSb samples grown by molecular beam epitaxy at different substrate temperatures. [35]
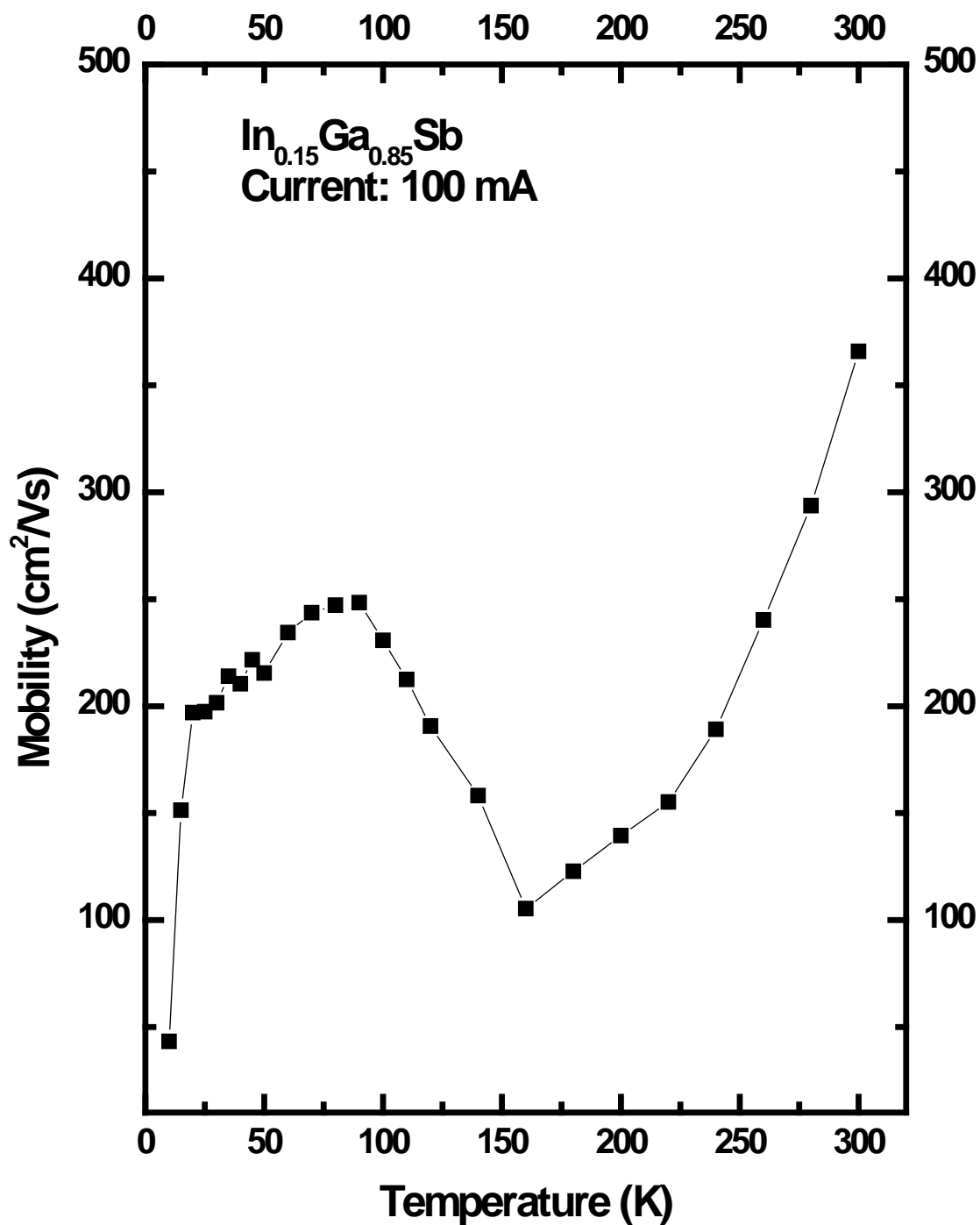
Figure 16. Hall mobility as a function of temperature from In$_{0.15}$Ga$_{0.85}$Sb using a current of 100 mA.

sample. This is a typical characteristic of impurity band conduction. Since there is no scattering

during the tunneling between adjacent impurities, the tunneling is essentially temperature

independent, and so is mobility in this temperature region. The impurity conductivity is also

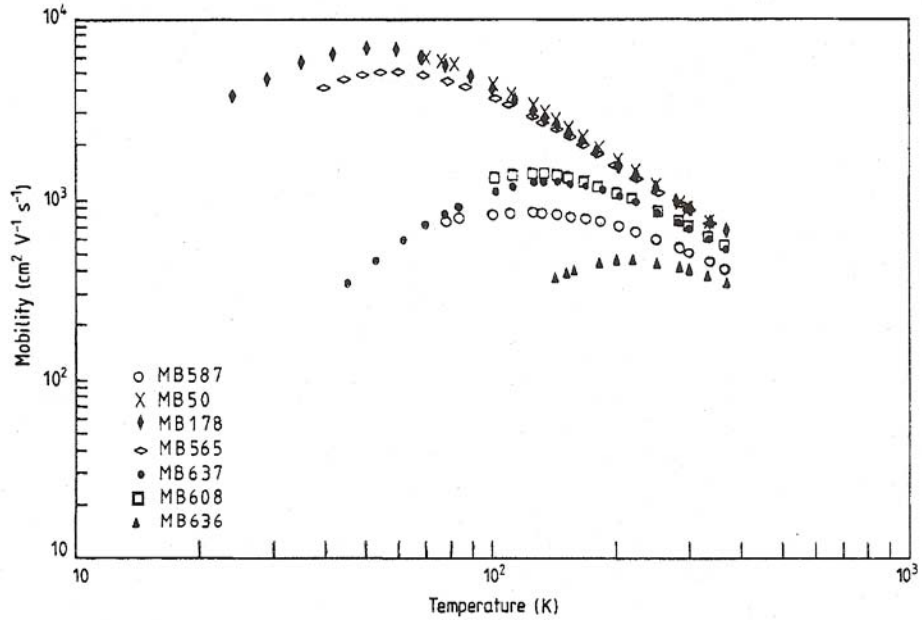almost temperature independent as shown in Fig. 12. As the temperature increases above 70 K,

the mobilities decrease due to lattice scattering. At above 160 K, the thermally ionized electrons

into the conduction band dominates, and the mobilities start to increase again due to impurity

screening. Here apparently the impurity scattering is dominant than the lattice scattering. As

mentioned in the conductivity discussion, carrier concentration is extremely dependent on

temperature. In one sample, Lee *et al*. found that the carrier concentration for InSb increased

from 5.8×10^{16} cm^{-3} at 77 K to 2.5×10^{17} cm^{-3} at 300 K, with even larger increases found at

different growth settings. [36] Fig. 17 shows the results of carrier concentrations as a function of

$1000/T$ (K^{-1}) for the In$_{0.15}$Ga$_{0.85}$Sb sample. The carrier concentration values ranged from 2×10^{17}

to 5×10^{17} cm^{-3}, and this sample is an n-type material. As can be seen in the figure, the carrier

concentration changes very much as temperature varies. The level of carriers remains relatively

constant in the temperature range from 20 to 50 K except for an unusually high carrier

concentration at 10 K and moderately high value at 15 K. The concentration decreases up to 90

K, increasing up to 160 K, and then decreases again as temperature increases up to 300 K.

The intrinsic carrier concentration was calculated by equation 4.2 [31]

$$n_i = 2 \left(\frac{2\pi \sqrt{m_n^* m_p^*} kT}{h^2} \right)^{3/2} e^{-\Delta\varepsilon/2kT}, \qquad (4.2)$$

where n_i is the intrinsic carrier concentration, m_n^* is the effective mass of the electrons, m_p^* is the

effective mass of the holes, k is Boltzmann's constant, 1.381×10^{-23} J/K, T is the temperature, h is

Planck's constant, and $\Delta\varepsilon$ is the band gap energy. Table 1 gives the values for the effective

24
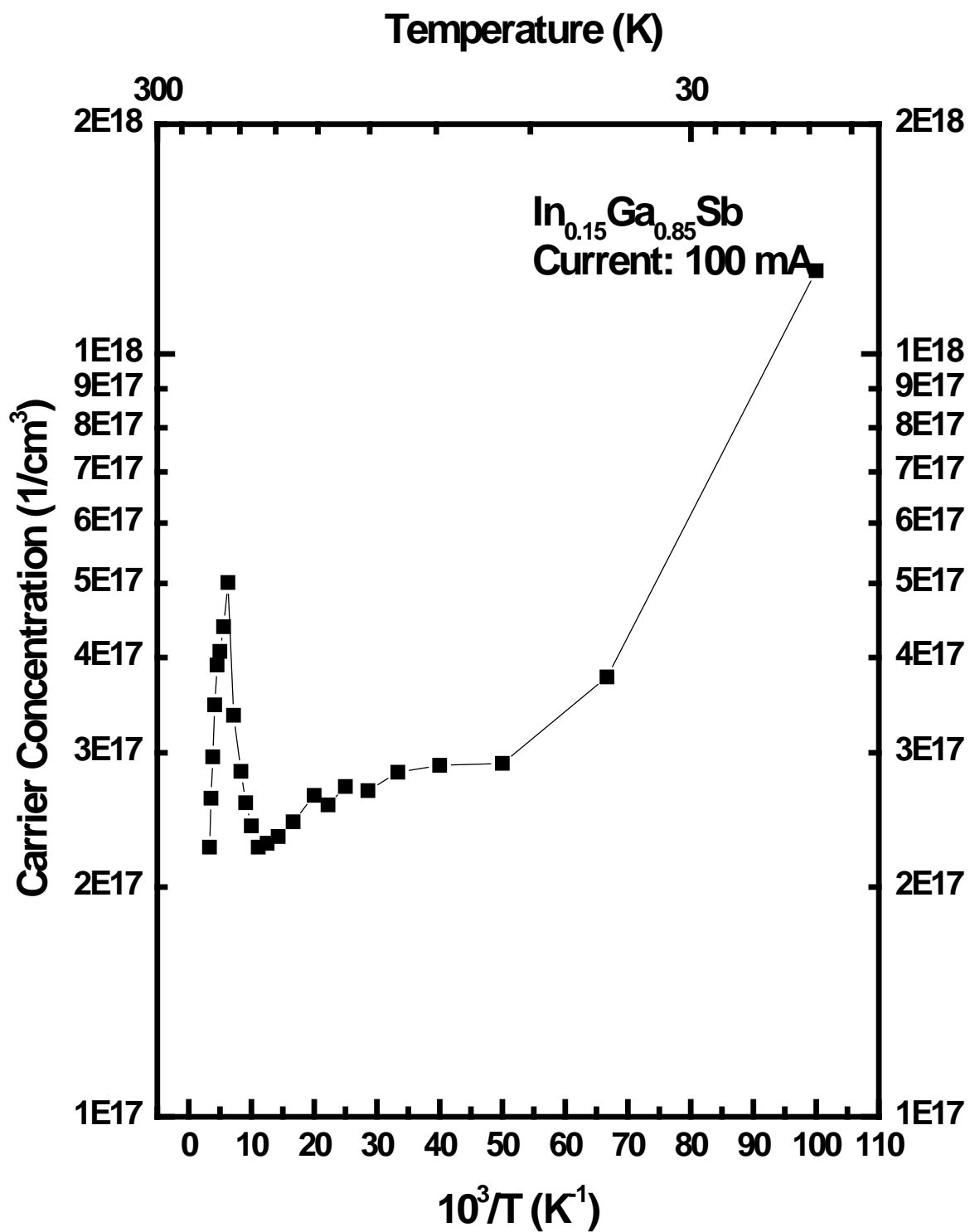
Figure 17. Carrier concentration as a function of inverse temperature from In$_{0.15}$Ga$_{0.85}$Sb using a current of 100 mA.

masses and the band gap energy for this material. Table 2 shows the intrinsic carrier

concentration from 10 to 300 K, and they are plotted in Fig. 18. As shown in the plot of the

intrinsic carrier concentration versus inverse temperature, the intrinsic carrier contribution for

this sample up to 300 K is negligible compared to the obtained carrier concentration. Therefore,

the effects of the intrinsic carriers are excluded for the temperature dependent carrier

concentration analysis.

Table 1. Effective masses and band gap energy of In$_{0.15}$Ga$_{0.85}$Sb.

Symbol	Value
m_n^*	$0.038 m_e$
m_p^*	$0.400 m_e$
$\Delta\varepsilon$	0.680 eV

Table 2. Intrinsic carrier concentrations for In$_{0.15}$Ga$_{0.85}$Sb as a function of temperature.

Temperature (K)	Intrinsic Carrier Concentration (cm^{-3})	Temperature (K)	Intrinsic Carrier Concentration (cm^{-3})
10	0	120	1.46×10^3
20	4.24×10^{-70}	140	2.02×10^5
30	2.75×10^{-41}	160	8.34×10^6
40	7.96×10^{-27}	180	1.54×10^8
50	4.08×10^{-18}	200	1.61×10^9
60	2.75×10^{-12}	220	1.12×10^{10}
70	4.15×10^{-8}	240	5.67×10^{10}
80	5.81×10^{-5}	260	2.26×10^{11}
90	1.66×10^{-2}	280	7.48×10^{11}
100	1.55	300	2.12×10^{-12}

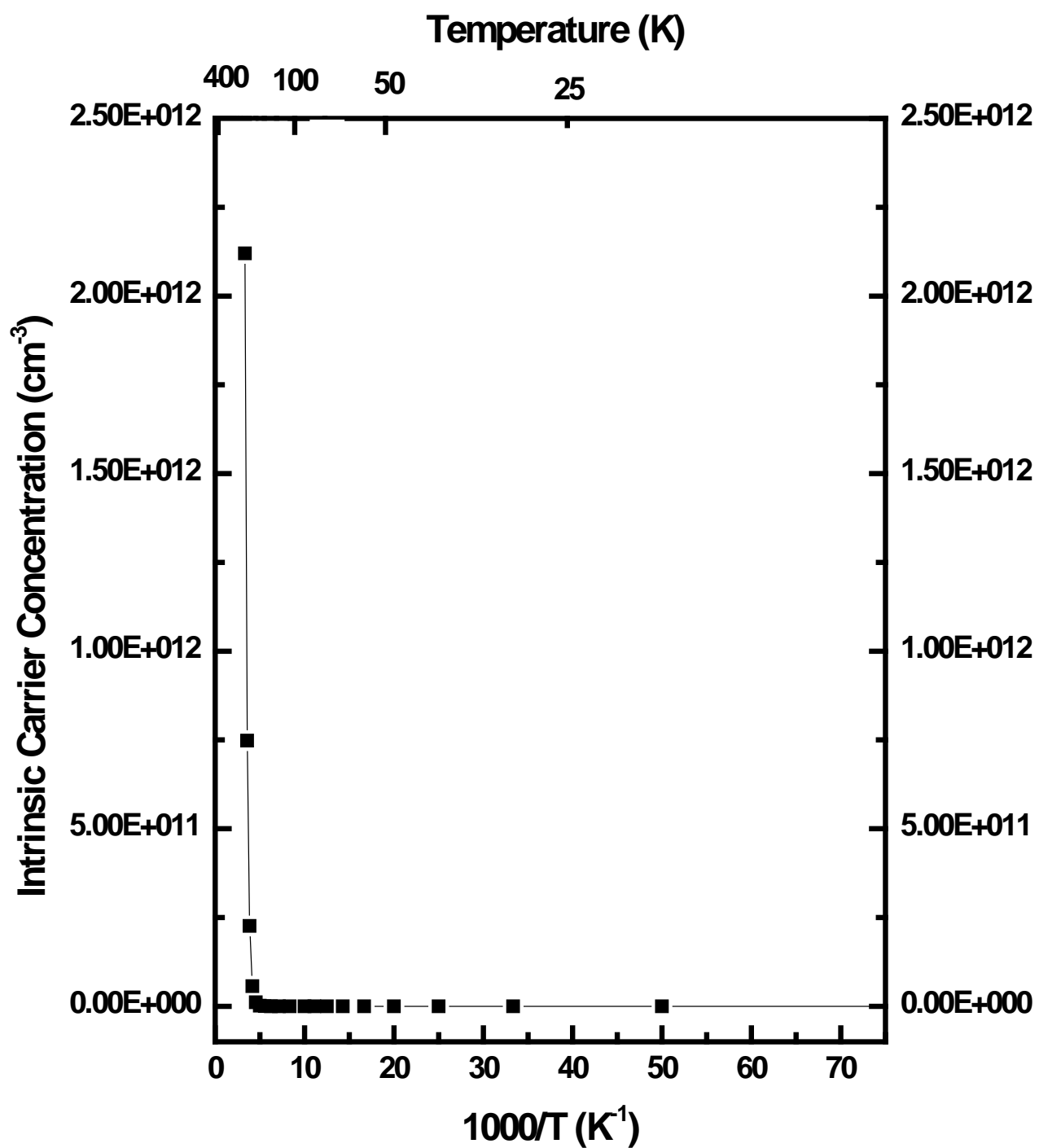**Figure 18. Intrinsic carrier concentration as a function of temperature for In$_{0.15}$Ga$_{0.85}$Sb.**

The explanation of temperature dependent carrier concentration is somewhat complicated, and it cannot be fully understood at present. The temperature dependent conductivity, mobility, and carrier concentration all seem to lead to the impurity band conduction at lower temperatures. For this impurity band conduction regime, conduction can occur either by tunneling from one impurity to the nearest neighboring impurity of the same type or after thermal excitation into the adjacent band for lesser doped material. Competition between these two processes is dependent on the temperature. At lower temperatures, it seems that the impurity band contributes to the carrier concentration, and above about 90 K, the impurities are thermally ionized causing increase in carrier concentrations. However, the decrease in carrier concentration above 160 K is not well understood at this point. Although carrier concentration fluctuates a lot with temperature, the conductivity type was maintained as n-type throughout the whole temperature range for this sample.

In the case of the $In_{0.80}Ga_{0.20}As$ sample, the Hall effect measurements were taken only at room temperature (275 K) and 77K. The conductivities obtained were 22.83 and 21.19 ohm^{-1}cm^{-1} for the sample temperatures of 77 and 295 K, respectively. The Hall mobilities obtained were 1.357×10^4 and 9.670×10^3 cm^2/V-s for the sample temperatures of 77 and 295 K, respectively. The carrier concentrations obtained were 1.063×10^{16} and 1.341×10^{16} cm^{-3} for the sample temperatures of 77 and 295 K, respectively. Since the temperature dependent Hall measurements were not taken, the detailed temperature dependent behavior cannot be described at present. However, the carrier concentration values, when compared to Oliver *et al.*'s study on $In_{0.47}Ga_{0.53}Sb$, almost an entire order of magnitude higher at room temperature and an even larger increase over their best sample at 77 K. [14] Unfortunately, the mobilities of the sample from this study were lower significantly lower than the mobilities found by Oliver *et al.* and Lideikis

et al. [14, 10] Using Eq. 2.1, Goldberg and Schmidt would have predicted the mobilities of

$In_{0.80}Ga_{0.20}As$ to be 2.58×10^4 cm^2/V-s. [26] As stated previously, impurities in a material will

decrease the mobility.

Results of Optical Characterization Data

The $In_{0.15}Ga_{0.85}Sb$ sample that was used in photoluminescence testing yielded consistent

results. Fig. 19 illustrates a simplified version of how the intensities of photoluminescence peaks

evolve as temperature changes. Fig. 20 shows photoluminescence studies made on $In_xGa_{1-x}Sb$

by Vankova *et al.* [1] It should be noted that Vankova *et al.*'s study on $In_xGa_{1-x}Sb$ produced two

distinct peaks, P_1 and P_2 (Fig. 20), which were a result of the band-to-band transistion and free

electron-neutral acceptor recombination, respectively. [28]
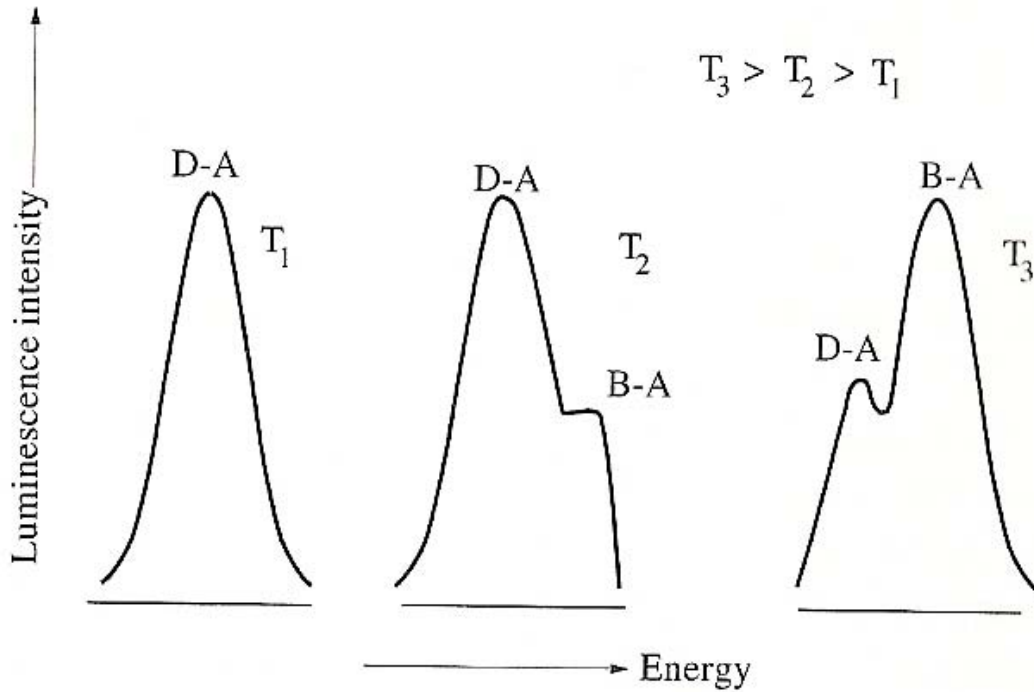
Figure 19. Schematic illustration of the evolution of band-acceptor and donor acceptor transitions at varying temperatures. [1]
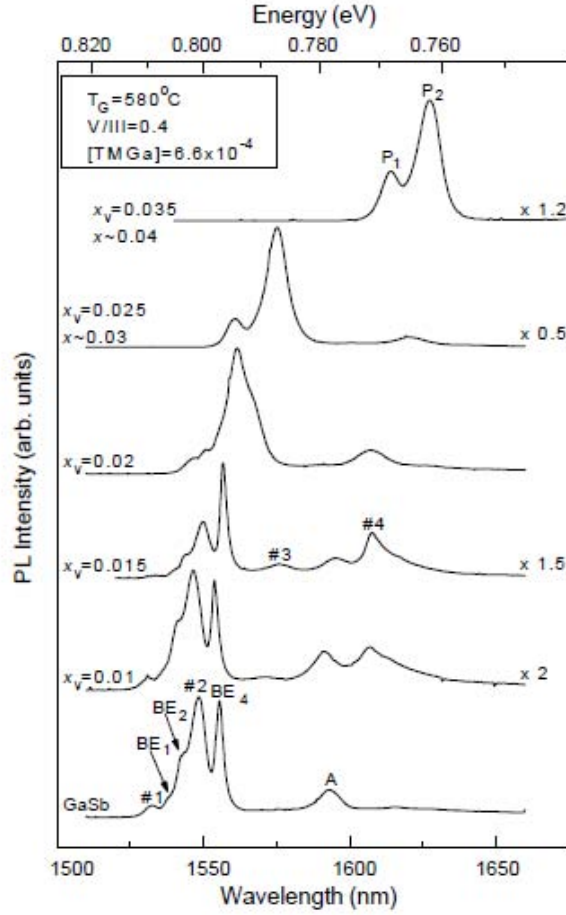
Figure 20. Vankova *et al.*'s photoluminescence results of In$_x$Ga$_{1-x}$Sb revealing two dominating peaks, P$_1$ and P$_2$. [28]

Photoluminescence data for In$_{0.15}$Ga$_{0.85}$Sb was taken at three different positions, labeled

A, B, and C. Data from location A will be discussed first. With the temperature at

approximately 12 K, laser power dependent data was obtained, and the results are shown in Fig.

21. It was found that there are two clear peaks and one shoulder peak located at 673, 649, and

628 meV, respectively. They are attributed to exciton bound to neutral acceptor, donor-shallow

acceptor, and donor-deep acceptor, respectively. As the laser power was increased from 50 mW

to 300 mW, the intensity of the luminescence also increased, as expected. However, above 300

mW the intensity began to drop. This is probably due to localized heating from the laser beam.

The relative intensity of the two peaks also changes with changing laser power. At low powers,

the peak at 673 meV dominates. As the power increases above 300 mW, the peak at 649 meV

eventually becomes the peak with the highest intensity. The shoulder at 628 meV is barely

observable at the lower powers, but at or above 300 mW, it is clearly distinguishable. It is

possible that this peak may have been due to longitudinal optical (LO) phonon replica, but it's

energy difference is only 21 meV, whereas LO phonon replica usually takes place at a difference

of approximately 29 meV.

The temperature dependent spectra taken at two laser powers of 240 and 475 mW are

shown in figures 22 and 23. The spectral intensity taken at both 12 and 30 K did not change

much at all for the lower laser power of 240 mW, whereas the photoluminescence intensity at 30

K for the 475 mW laser power decreased considerably from that at 12 K due to additional local

laser heating. From Fig. 22, it can be observed that the peak intensity at 675 meV decreases

more rapidly compared with that at 652 meV. Therefore, the peak at 675 meV is assigned as

exciton bound to neutral acceptor because this bound exciton dissociates much quicker than the

donor-acceptor peak. Also, it can be observed that the photoluminescence spectrum intensities

for a laser power of 475 mW decreases more rapidly as temperature increases compared to those

for 240 mW laser power. It should be noted that the spectra obtained at higher laser powers

during this study might be influenced by localized heating to some extent due to the high laser

power. This can be noticed more clearly by comparing temperature dependent and laser power

dependent spectra shown in figures 21-23. That is, the spectral intensity and shape observed at

12 K with 570 mW shown in Fig. 21 is very similar to those observed at 50 K with 240 mW and

at 30 K with 475 mW.
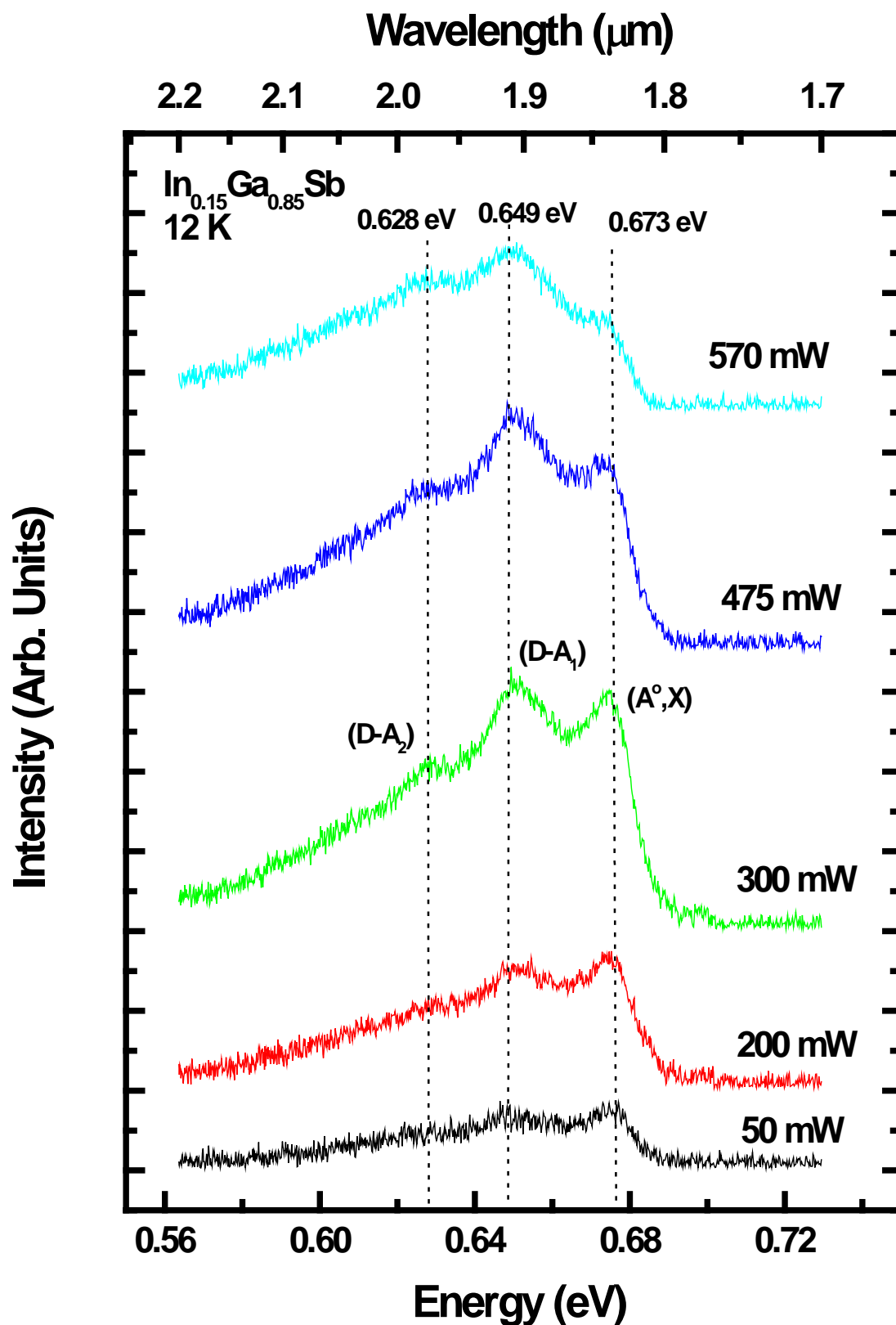
Figure 21. PL data for In$_{0.15}$Ga$_{0.85}$Sb taken at 12 K on location A.

Figure 22. PL data for In$_{0.15}$Ga$_{0.85}$Sb taken on location A using a laser power of 240 mW.

Figure 23. **PL data for In$_{0.15}$Ga$_{0.85}$Sb taken on location A using a laser power of 475 mW.**

Figure 24 shows the photoluminescence spectra taken at 13 K with different laser powers at location B. A new clear peak at 701 meV is observed at this position as shown in this figure. However, this peak is attributed to a laser plasma line due to the fact that it does not change positions with varying temperature and laser power. In Fig. 24, it can also be seen that the donor-shallow acceptor peak intensity at 651 meV is nearly saturated after exciting with 300 and 475 mW, and its intensity decreases after increasing the laser power above 475 mW. Fig. 25 shows photoluminescence spectra taken at a laser power of 475 mW as a function of temperature. The exciton bound to neutral acceptor peak at 675 meV, donor-shallow acceptor peak at 650 meV, and donor-deep acceptor peak at 629 meV are observed similar to Fig. 23.

Fig. 26 displays data taken at location C on the $In_{0.15}Ga_{0.85}Sb$ sample at 13 K with varying laser power. The shoulder peak at 628 meV that was present at locations A and B is also present at location C. It has been observed that there are double peaks centered at 654 meV. The origins or reasons are not understood at present. Fig. 27 shows the temperature dependent data taken on location C with the laser power set at 475 mW.

Figures 28 and 29 show how the spectra for each location changes at the sample temperatures of 12 and 30 K. All three peak positions are observed at the same photon energy for the data taken at 12 K, but the bound exciton peaks observed at 30 K from locations B and C shifted to a slightly higher energy compared to that from location A. Also the photoluminescence intensity at location B is in general much stronger compared with that at location A or C. Other than those differences indicated, the photoluminescence observed from the three locations indicate that the crystal quality and indium composition of the whole sample is fairly uniform.
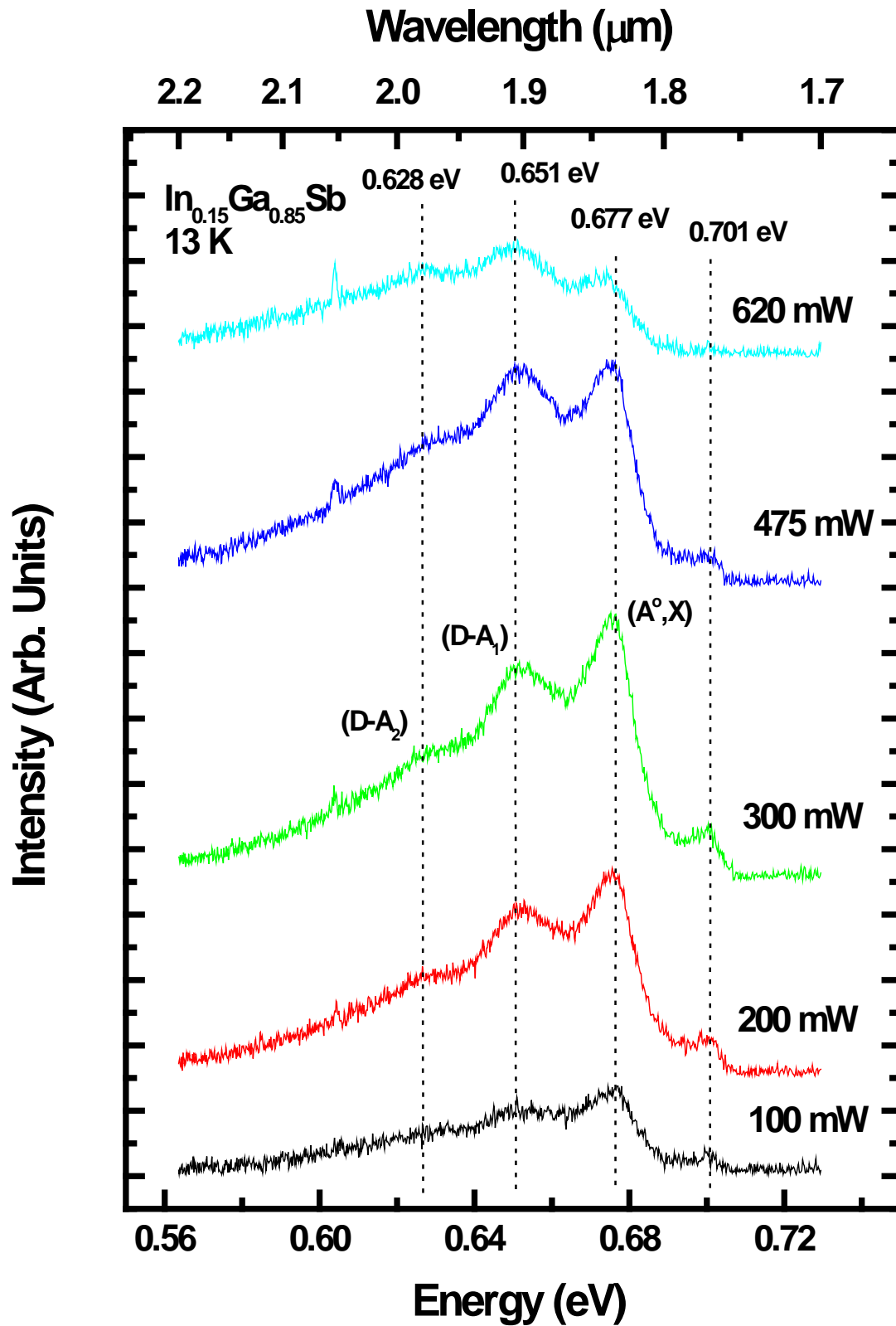
Figure 24. PL data for $In_{0.15}Ga_{0.85}Sb$ taken at 13 K on location B.
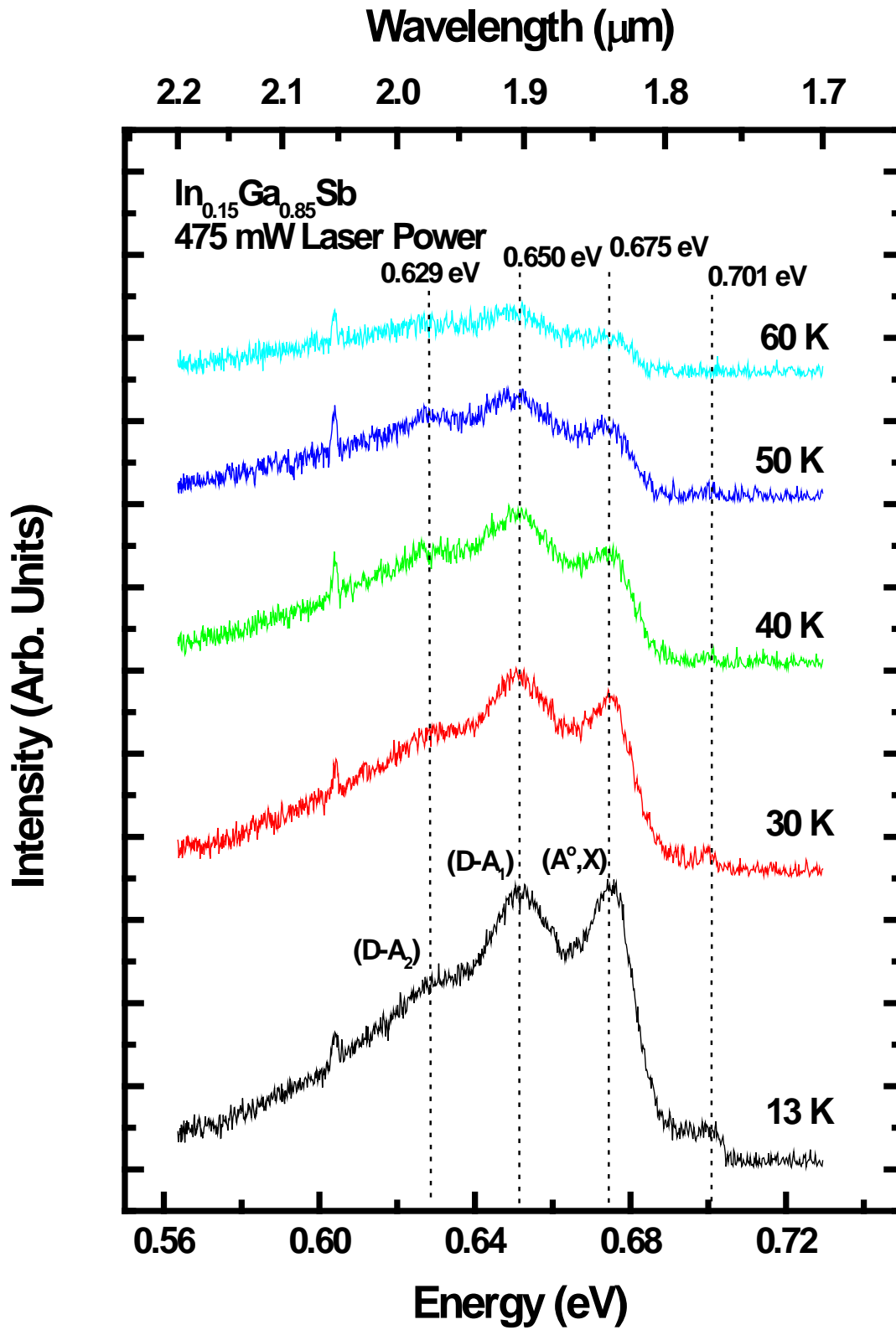
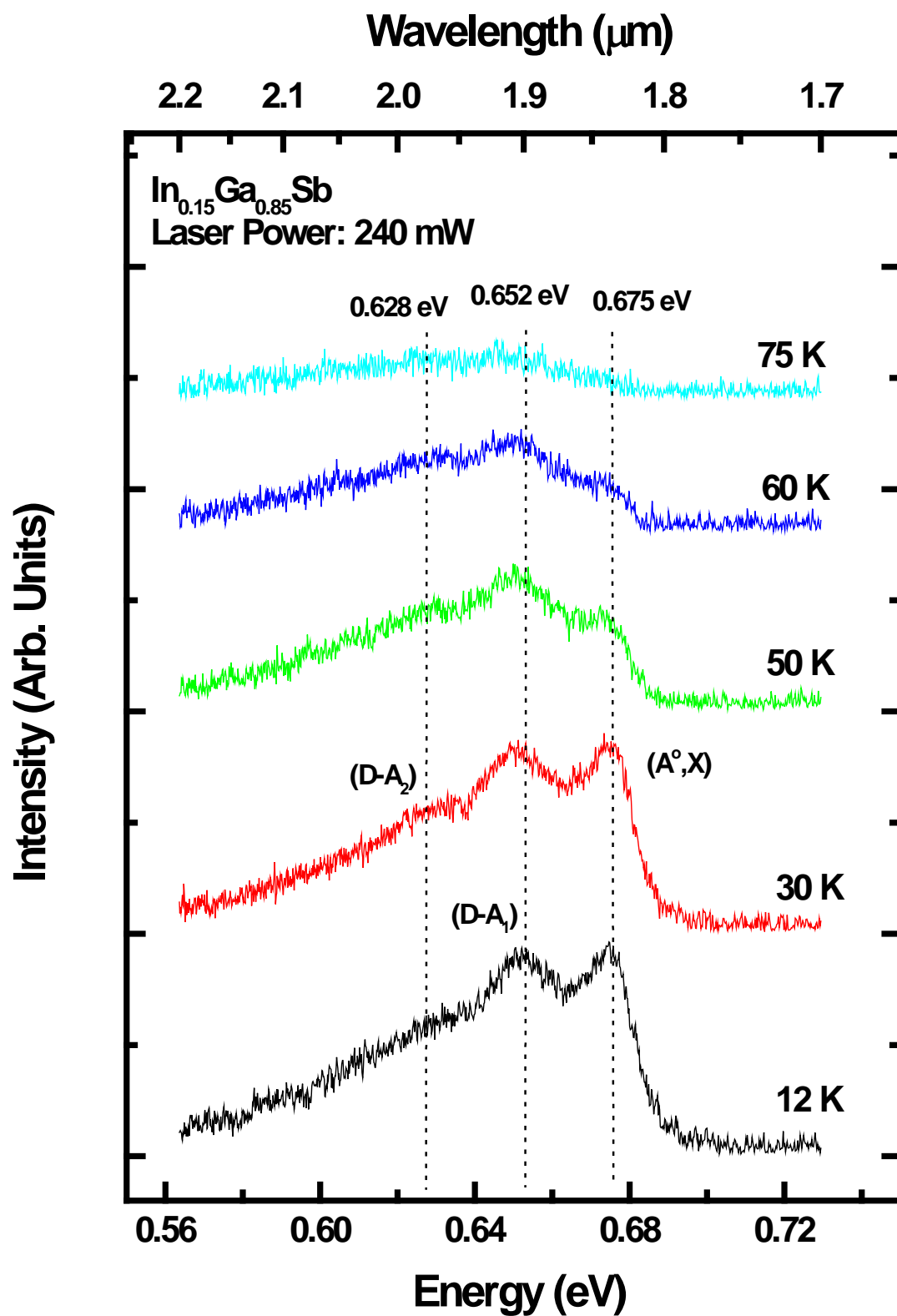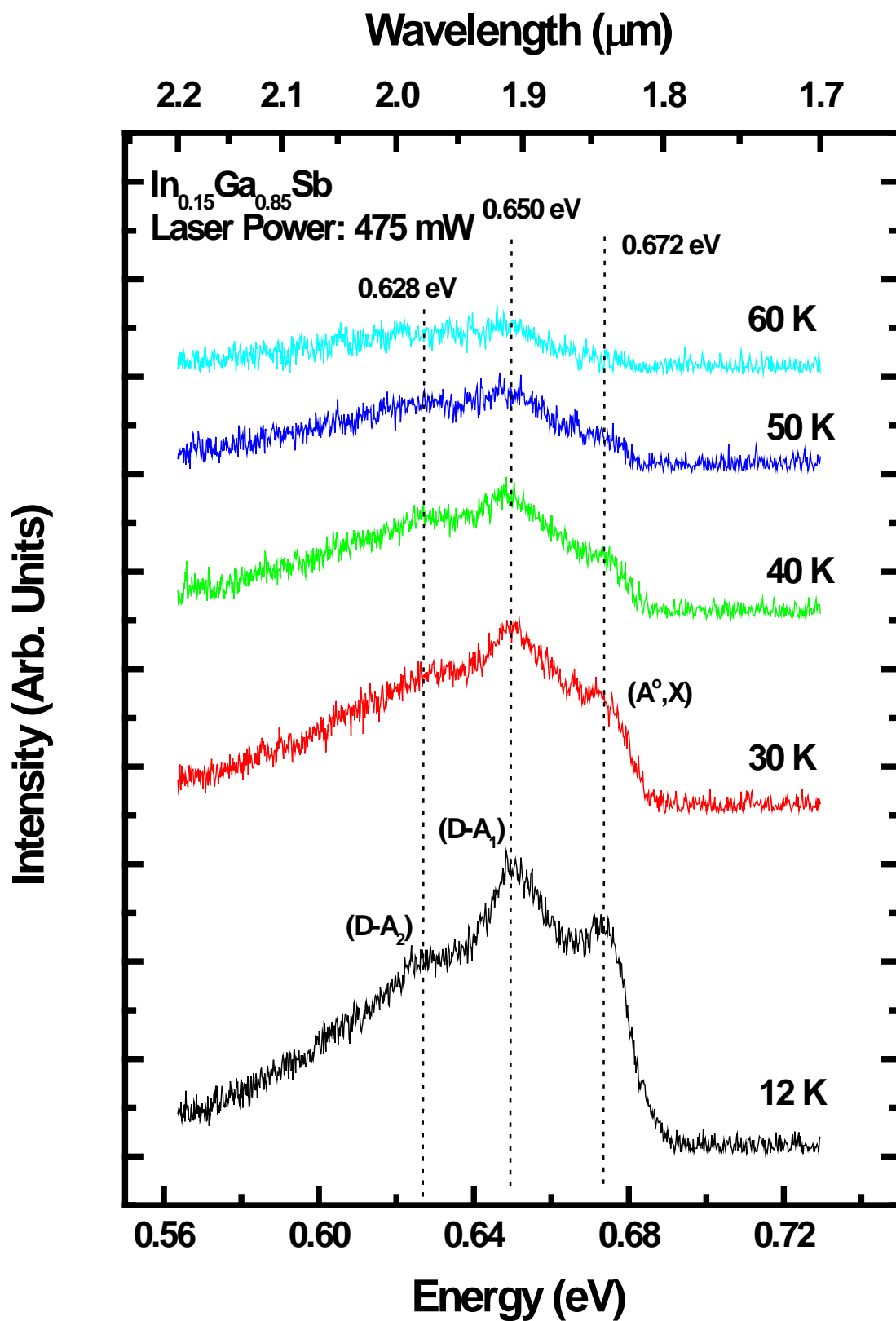**Figure 25.** PL data for $In_{0.15}Ga_{0.85}Sb$ taken on location B using a laser power of 475 mW.
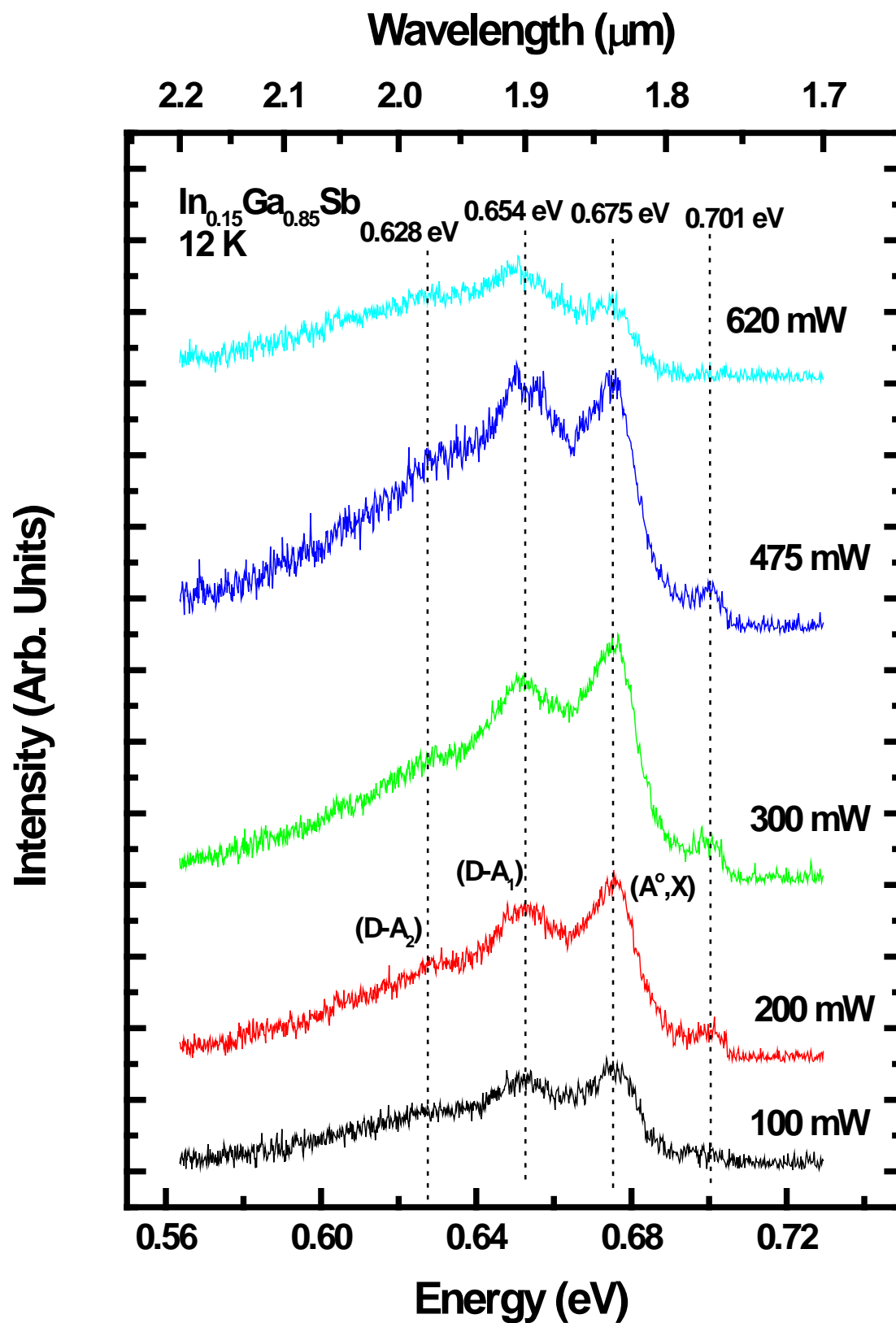
Figure 26. PL data for $In_{0.15}Ga_{0.85}Sb$ taken at 12 K on location C.
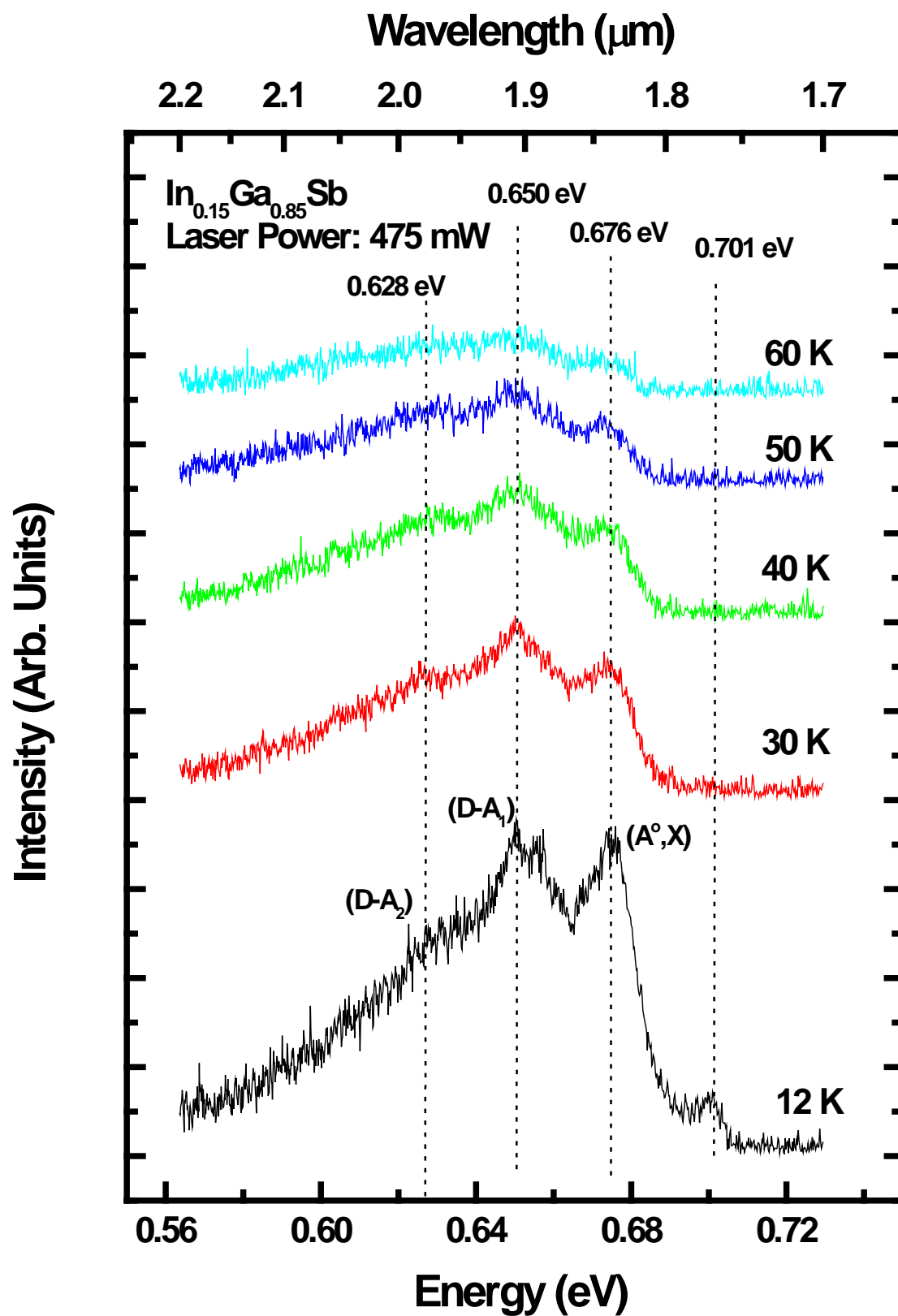
Figure 27. PL data for $In_{0.15}Ga_{0.85}Sb$ taken on location C using a laser power of 475 mW.
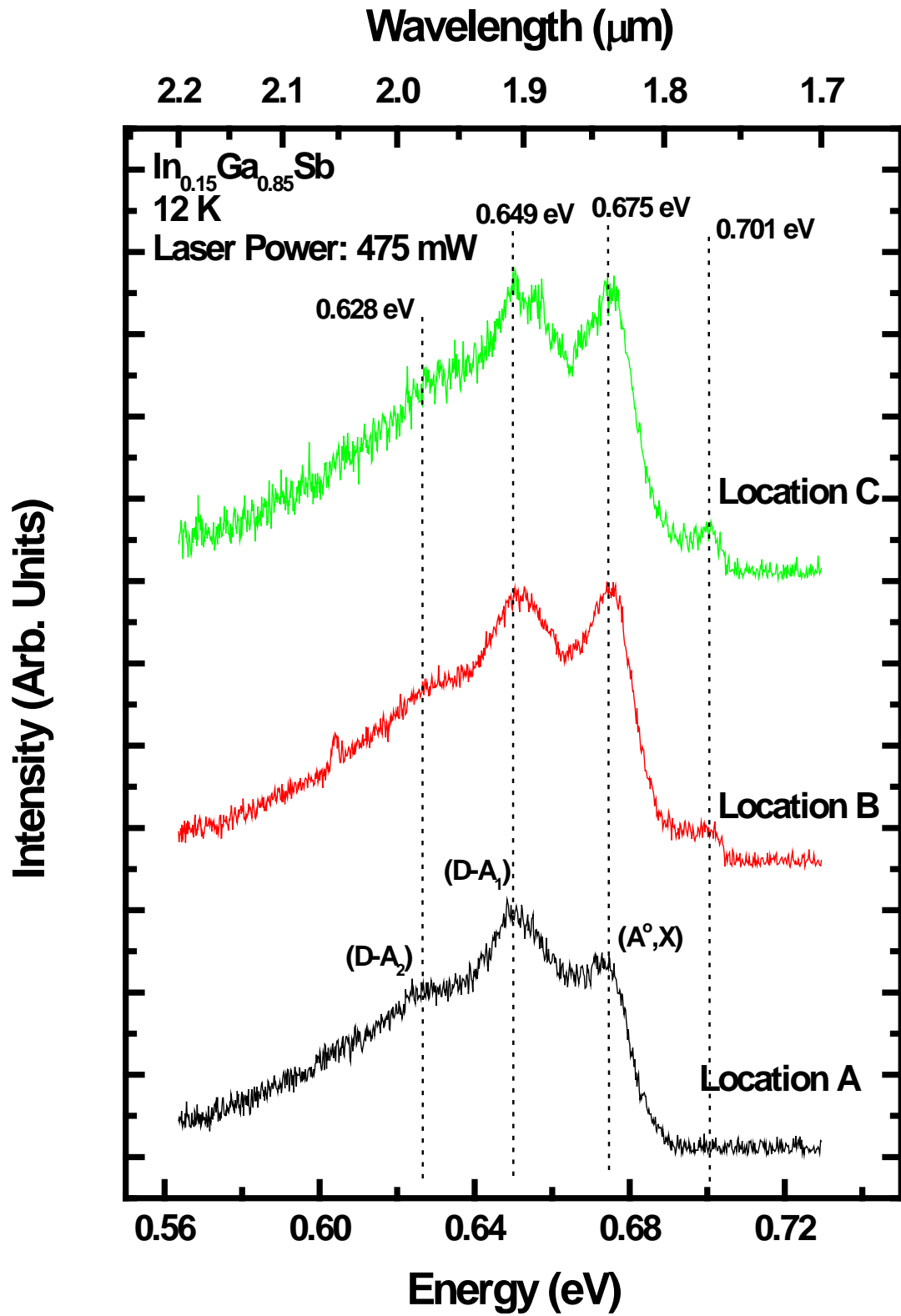
Figure 28. PL data for In$_{0.15}$Ga$_{0.85}$Sb taken on locations A, B, and C at 12 K with the laser power set to 475 mW.
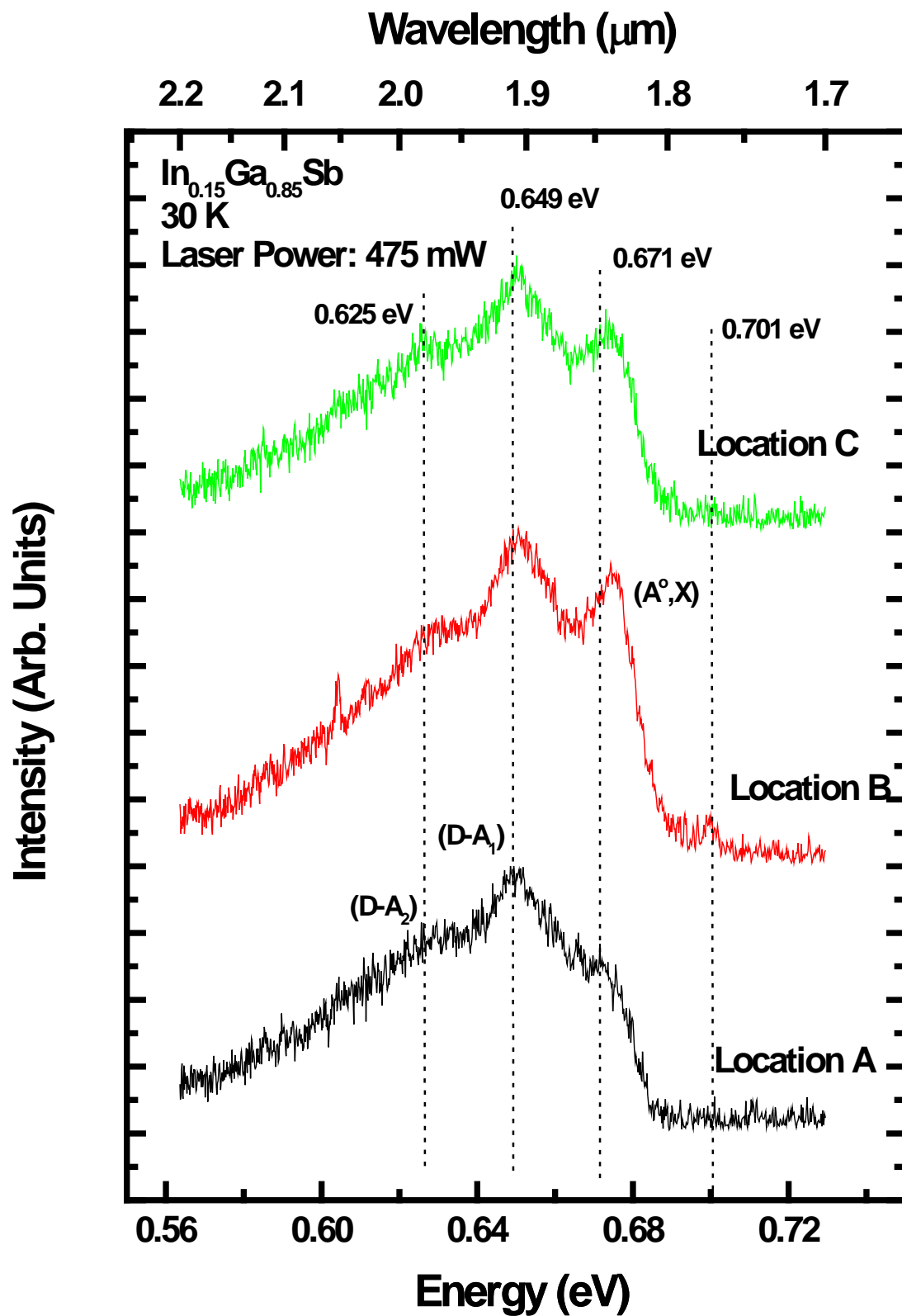
Figure 29. PL data for $In_{0.15}Ga_{0.85}Sb$ taken on locations A, B, and C at 30 K with the laser power set to 475 mW.

One phenomenon that occurs in semiconductor materials is a "blue shift" in band gap peak as the sample temperature decreases. This can be seen in Vankova *et al.*'s data for $In_{0.025}Ga_{0.975}Sb$ and $In_{0.015}Ga_{0.985}Sb$ samples as shown in Fig. 30. The shift to a higher band gap energy can be explained by multiple effects, including an increase in the interatomic spacing due to the thermal energy increasing in the material. The electronic bands are formed by overlapping of the wave functions and when the interatomic spacing is altered, the wave function overlapping is also changed. Equation 4.2, known as the Varshni relation, gives an approximation of the temperature dependence of the energy band gap for a given material [37]

$$E_g(T) = E_g(0) - \frac{\alpha T^2}{T + \beta}.$$ (4.2)

In Equation 4.2, α and β are material specific constants. In general, α is near 0.5 and β is approximately the Debye temperature, which is the highest temperature that can be achieved through a single normal vibration from a phonon. [37] The luminescence spectra obtained from the current $In_{0.15}Ga_{0.85}Sb$ sample do not clearly show the effect of this shift in energy band gap as
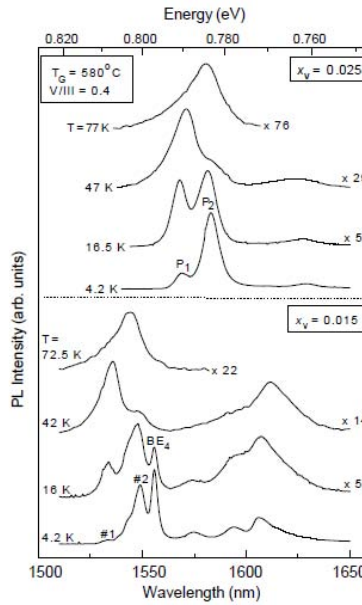
Figure 30. Temperature dependent data showing shift in band gap energy peaks as temperature increases.

temperature increases. The shift would more than likely be detected with further increase in temperature. However, before seeing the band gap change effect in photoluminescence signal, the luminescence signal became too weak to obtain a strong enough signal to noise ratio as the temperature reached approximately 75 K.

$In_{0.80}Ga_{0.20}As$ was also subject to photoluminescence testing. Fig. 31 shows the photoluminescence spectra taken at 10 K as a function of laser power from location A. It shows a single broad peak at 572 meV, which is believed to be a band-to-band transition. Some evidence of band filling appears on the high energy side of the peak at 572 meV. As with the $In_{0.15}Ga_{0.85}Sb$ sample, there are localized heating effects at higher laser powers that will skew the data slightly as shown in Fig. 31. In this figure, there is a shoulder peak that is present at approximately 550 meV, which is attributed to the donor-acceptor transition that occurs at an energy 22 meV below the gand gap energy. This shoulder is quenched by the time the laser power is increased to 400 mW. The peak at 604 meV is due to a laser plasma line. Figures 32 and 33 show the photoluminescence spectra taken as a function of temperature at 300 mW of laser power from locations B and C, respectively. In all cases, the blue shift can be observed as the temperature decreases. The shift is approximately 30 meV with a decrease in temperature of approximately 120 K (0.25 meV/K). The shoulder is barely observable at location B taken at 12 K, as shown in Fig. 32. For this sample, the band to band peaks appear at 562, 548, and 534 meV for the locations of A, B, and C, respectively, for the data taken at 10 K with 300 mW. Certainly, the photoluminescence peak position shows location dependence and this might indicate that the indium molar fraction may be slightly different throughout the sample.
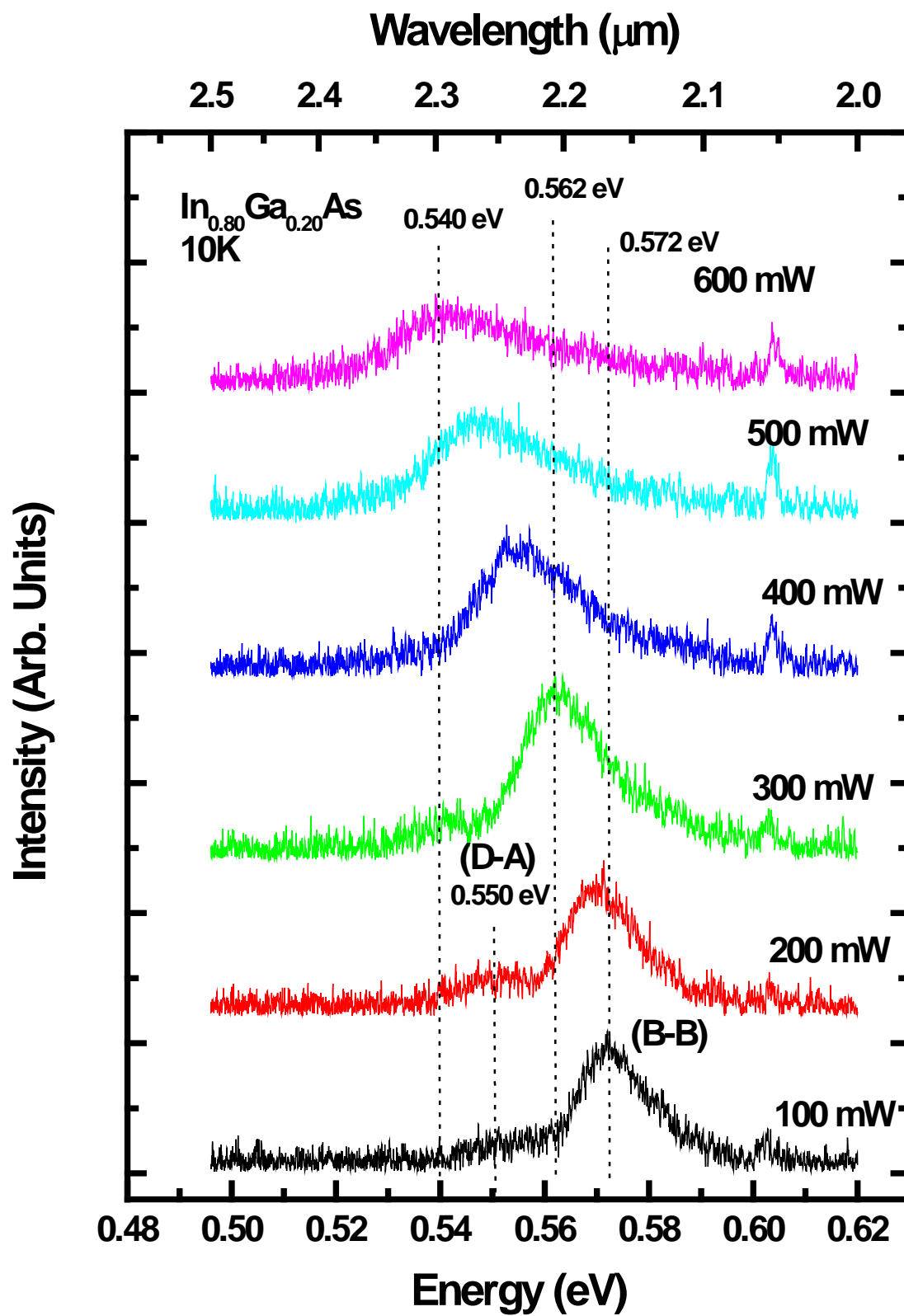
Figure 31. PL data for In$_{0.80}$Ga$_{0.20}$As taken at 10 K on location A.
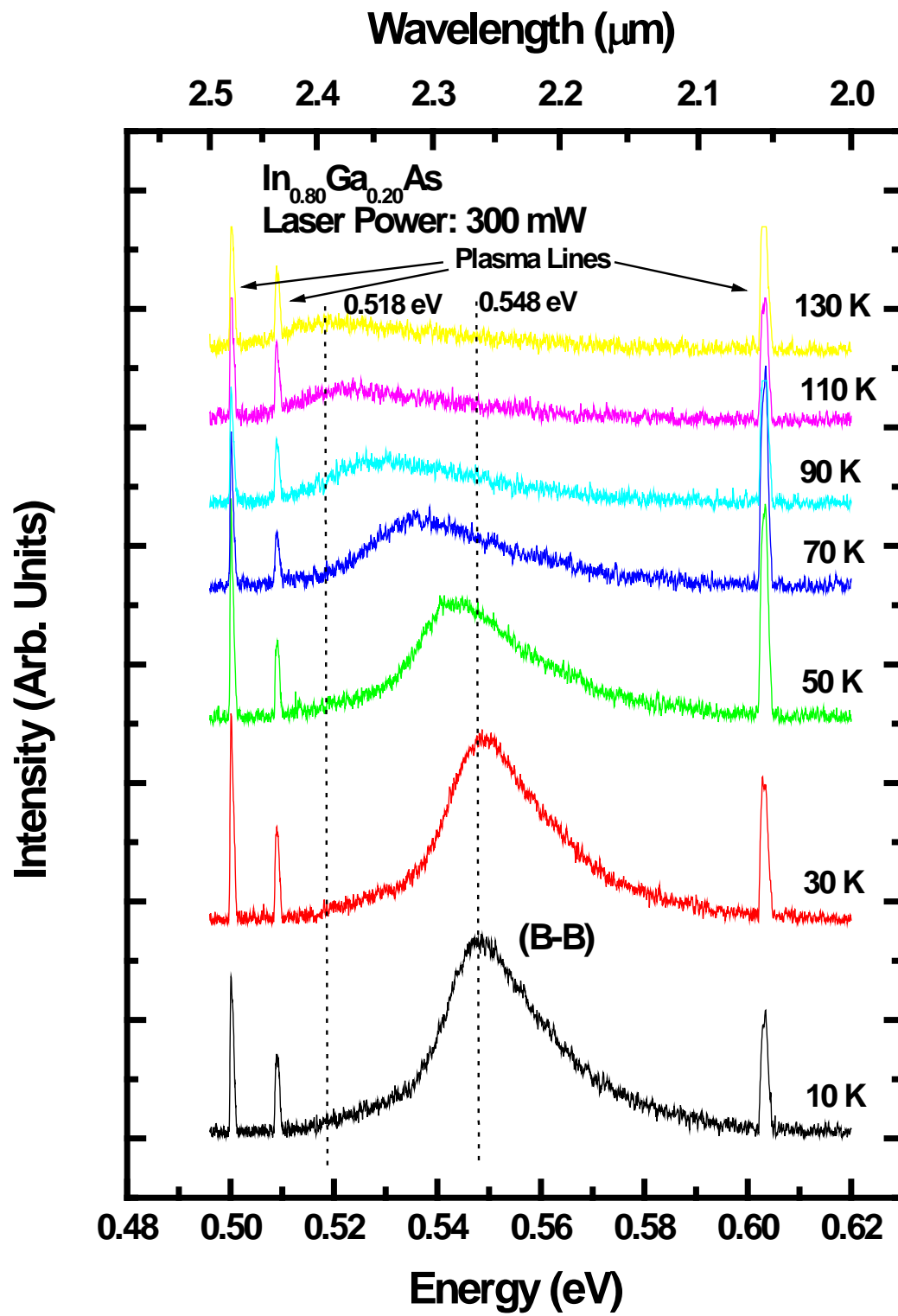
Figure 32. PL data for In$_{0.80}$Ga$_{0.20}$As taken on location B using a laser power of 300 mW.
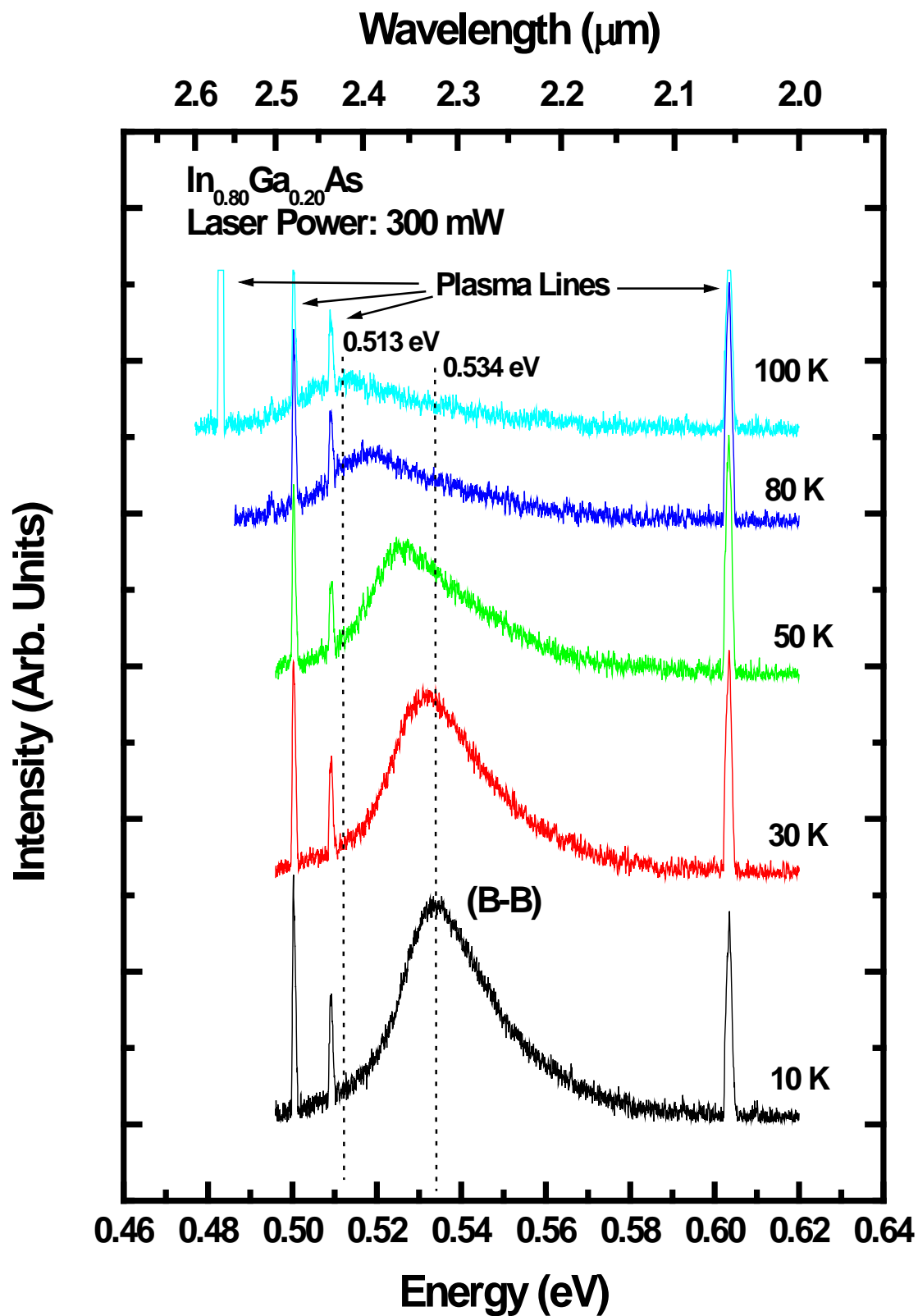
Figure 33. PL data for In$_{0.80}$Ga$_{0.20}$As taken on location C using a laser power of 300 mW.

Summary

The $In_{0.15}Ga_{0.85}Sb$ sample's electrical characterization data shows a clear trend in temperature dependence of carrier concentration, mobility, and conductivity. It produced valuable photoluminescence data that was useful in evaluating the homogeneity of a bulk grown sample.

The $In_{0.80}Ga_{0.20}As$ sample provided consistent Hall effect data that was used to determine electrical characteristics of the material. It also produced constructive photoluminescence data, which show a clear shift in the band gap energy as a function of temperature.

V. Conclusions and Recommendations

The results of photoluminescence (PL) study for the $In_{0.15}Ga_{0.85}Sb$ sample show an exciton bound to neutral acceptor (A^o,X) transition at 675 meV, a donor-shallow acceptor pair (D-A_1) transition at 650 meV, and a donor-deep acceptor pair (D-A_2) transition at 628 meV, and they provide useful data in verifying the band gap energy of the material and estimating acceptor and donor levels. Assuming a binding energy of the (A^o,X) is 5 meV would yield a band gap energy of 680 meV, which is consistent with the result of 670 meV estimated from the transmission measurements. Typical donor energy level in GaSb is around 3 meV, and thus the shallow acceptor level would be around 27 meV, and the deep acceptor level would be around 49 meV. The Hall-effect measurements show that this sample is n-type material with a room temperature carrier concentration of about $4x10^{17}/cm^3$. The mobility obtained at room temperature is about 300 cm^2/V•s, which is very low compared with the typical value of electron mobility of 5000 cm^2/V•s for GaSb at room temperature. While the current bulk grown ternary alloy material may not be great yet for direct use in next generation devices, it will provide a suitable substrate for which to grow epitaxial layers.

The $In_{0.80}Ga_{0.20}As$ is n-type material with a room temperature carrier concentration of $1.34x10^{16}/cm^3$ and mobility of 9,670 cm^2/V•s. This mobility is much lower than expected when compared with the typical electron mobility for InAs of 33,000 cm^2/V•s. The PL results of this sample shows a broad band to band peak at 572 meV, which is consistent with the result of 574 meV estimated from the transmission measurements. The band to band photoluminescence was observed to shift peak position, indicating a slight inhomogeneity in indium mole fraction.

Recommendations

The photoluminescence experimental setup can be improved by using a faster optical lens following the sample chamber. A lens with a shorter focal length, such as 50 mm, can be placed closer to the sample chamber and will therefore gather more of the emitted photons from the material. Also, a Fourier transform infrared spectrometer may provide better data due to its ability to detect weak signals.

This research could be complimented by gathering data on $In_xGa_{1-x}Sb$ and $In_xGa_{1-x}As$ samples with a wider range of indium mole fractions. Collecting the mole fraction dependent data can be modeled, and the results of these bulk grown materials can be compared with those of the epitaxial grown materials. In addition, a 514 nm notch filter would be beneficial when conducting the photoluminescence measurements to remove all laser plasma lines. This would ensure any observed peaks are not a result of the plasma lines. Also, the photoluminescence measurements would benefit from placing a molybdenum mounting plate between the copper cold finger and the sample in order to reduce temperature effects experienced at low temperatures. Electron paramagnetic resonance spectroscopy measurements would aid in identifying any impurities within the sample.

Bibliography

1. P. Battacharya, *Semiconductor Optoelectronic Devices*, 2nd Ed. Prentice Hall, 1997.

2. C. Snyder, B. Orr, D. Kessler, and L. Sander, "Effect of Strain on Surface Morphology in Highly Strained InGaAs Films," *Physical Review Letters*, vol. 66, no. 23, pp. 3032-3035, 1991.

3. K. Okamoto, R. Hananoki, and K. Sakiyama, "InGaAs Epilayers of High In Composition Grown on GaAs Substrates by Molecular Beam Epitaxy," *Japanese Journal of Applied Physics*, vol. 33, part 1, no. 1A, pp. 28-32, 1994.

4. K. Okamoto, H. Tosaka, K. Yamaguchi, "Profiling of Double Crystal X-Ray Diffraction of InGaAs Epilayers Grown on GaAs," *Japanese Journal of Applied Physics*, vol. 30, no. 6, pp. 1239-1242, 1991.

5. Important Issues on Film Deposition. http://www.southalabama.edu/engineering/ece/faculty/akhan/Courses/EE539-439-s04/Lectures%20slides/Lecture%2021%20thinfilm%20deposition-LPCVDchapter%209.pdf Accessed 2 Feb 2009.

6. H. Wang and G. Ng, "Electrical Properties and Transport Mechanisms of InP/InGaAs HBTs Operated at Low Temperature," *IEEE Transactions on Electron Devices*, vol. 48, no. 8, pp. 1492-1497, 2001.

7. R. Mirin, J. Ibbetson, K. Nishi, A. Gossard, and J. Bowers, "1.3 μm photoluminescence from InGaAs quantum dots on GaAs," *Applied Physics Letters*, vol. 67, no. 25, pp. 3795-3797, 1995.

8. S. Wang, W. Wang, H. Zhu, L. Zhao, R. Zhang, F. Zhou, H. Shu, and R. Wang, "MOVPE growth of grade-strained bulk InGaAs/InP for broad-band optoelectronic device applications," *Journal of Crystal Growth*, vol. 260, pp. 464-468, 2004.

9. K. Nishi, H. Saito, and S. Sugou, "A narrow photoluminescence linewidth of 21 meV at 1.35 μm from strain-reduced InAs quantum dots covered by $In_{0.2}Ga_{0.8}As$ grown on GaAs substrates," *Applied Physics Letters*, vol. 74, no. 8, pp. 1111-1113, 1999.

10. T. Lideikis, K. Naudzlus, G. Treideris, A. Krotkus, and K. Grigoras, "Picosecond GaAs and InGaAs photoconductive switches obtained by low-temperature metal-organic chemical vapour deposition," *Semiconductor Science Technology*, vol. 7, pp. 845-849, 1992.

11. J. Faist, F. Capasso, D. Sivco, A. Hutchinson, S. Chu, A. Cho, "Short wavelength ($\lambda \sim 3.4$ µm) quantum cascade laser based on strained compensated InGaAs/AlInAs," *Applied Physics Letters*, vol. 72, no. 6, pp. 680-682, 1998.

12. T. Kim, T. Ghong, Y. Kim, S. Kim, D. Aspnes, T. Mori, T. Yao, and B. Koo, "Dielectric functions of $In_xGa_{1-x}As$ alloys," *Physical Review* B, vol. 68, no. 115323, pp. 1-10, 2003.

13. R. Pritchard, N. Collis, B. Hamilton, J. Thompson, N. Carr, and A. Wood, "Composition assessment of spatially resolved photoluminescence of InGaAs and InGaAsP epilayers grown on recessed InP substrates," *Semiconductor Science Technology*, vol. 8, pp. 1166-1172, 1993.

14. J. Oliver, Jr., L. Eastman, P. Kirchner, and W. Schaff, "Electrical Characterization and Alloy Scattering Measurements of LPE $Ga_xIn_{1-x}As$/InP for High Frequency Device Applications," *Journal of Crystal Growth*, vol. 54, pp. 64-68, 1981.

15. H. Yamaguchi, R. Dreyfus, and Y. Hirayama, "Excellent electric properties of free-standing InAs membranes," *Applied Physics Letters*, vol. 78, no. 16, pp. 2372-2374, 2001.

16. Y. Nishijima, K. Nakajima, K. Otsubo, and H. Ishikawa, "InGaAs Bulk Crystal Growth for High T_0 Semiconductor Lasers," *IEEE Proceedings*, 10th International Conference on Indium Phosphide and Related Materials, pp. 45-48. 11-15 May 1998.

17. Y. Gao, H. Kan, J. Murata, M. Aoyama, and T. Yamaguchi, "High Purity $In_xGa_{1-x}Sb$ Single Crystals with Cutoff Wavelength of 7-8 µm Grown by Melt Epitaxy," *Journal of Electronic Materials*, vol. 29, no. 10, pp. L25-L27, 2000.

18. T. Rafaat, M. Abedin, U. Singh, V. Bhagwat, I. Bhat, and P. Dutta, "Characterization of InGaSb Detectors for 1.0 to 2.4 µm Applications," *Proceedings of SPIE*, vol. 5406, pp. 56-63, 2004.

19. A. Bignazzi, E. Grilli, M. Guzzi, M. Radice, A. Bosacchi, S. Franchi, and R. Magnanini, "Low temperature photoluminescence of tellurium-doped GaSb grown by molecular beam epitaxy," *Journal of Crystal Growth*, vol. 169, pp. 450-456, 1996.

20. E. Glaser, R. Magno, B. Shanabrook, and J. Tischler, "Optical characterization of $In_{0.27}Ga_{0.73}Sb$ and $In_xAl_{1-x}As_ySb_{1-y}$ epitaxial layers for development of 6.2-A-based heterojunction bipolar transistors," *Journal of Vacuum Science Technology* B, vol. 24, no. 3, pp. 1604-1606, 2006.

21. M. Chioncel, C. Diaz-Guerra, J. Piqueras, N. Duhanian, and T. Duffar, "Assessment of IngaSb Crystals by Cathodo-luminscence Microscopy and Spectroscopy," *Journal of Optoelectronics and Advanced Materials*, vol. 6, no. 1, pp. 237-241, 2004.

22. A. Chandola, H. Kim, P. Dutta, "Below band-gap optical absorption in $Ga_xIn_{1-x}Sb$ alloys," *Journal of Applied Physics*, vol. 98, no. 093103, pp. 1-7, 2005.

23. G. Petty, *A First Course in Atmospheric Radiation*, Sundog Pub., 2004.

24. J. Woolley and C Gillett, "Electrical Properties of GaSb-InSb Alloys," *Journal of Physical Chemistry of Solids*, vol. 17, nos. 1/2, pp. 34-43, 1960.

25. R. Magno, E. Glaser, B. Tinkham, J. Champlain, J. Boos, M. Ancona, and P. Campbell, "Narrow band gap InGaSb, InAlAsSb alloys for electronic devices," *Journal of Vacuum Science Technology* B, vol. 24, no. 3, pp. 1622-1625, 2006.

26. Y. Goldberg and N. Schmidt, *Handbook on Semiconductor Parameters*, vol. 2, World Scientific, 1999.

27. J. Thobel, L. Baudry, A. Cappy, P. Bourel, and R. Fauquembergue, Electron transport properties of strained $In_xGa_{1-x}As$," *Applied Physics Letters*, vol. 56, no. 4, pp. 346-348, 1990.

28. V. Vankova, A. Leitch, and J. Botha, "Photoluminescence characterization of unintentional acceptors in MOVPE-grown GaInS," *Journal of Crystal Growth*, vol. 248, pp. 279-283, 2003.

29. H. Matsuura, K. Nishikawa, M. Segawa, and W. Susaki, "Accurate Determination of Acceptor Densities and Acceptor Levels in Undoped InGaSb from Temperature Dependence of Hole Concentration," *Japanese Journal of Applied Physics*, vol. 45, no. 8A, pp. 6373-6375, 2006.

30. Z. Fang, K. Ma, D. Jaw, R. Cohen, and G. Stringfellow, "Photoluminescence of InSb, InAs, and InAsSb grown by organometallic vapor phase epitaxy," *Journal of Applied Physics*, vol. 67, no. 11, pp. 7034-7039, 1990.

31. J. McKelvey, *Solid State Physics for Engineering and Materials Science*, Krieger Publishing Company, 2003.

32. G. Gruen, "Time Dependent Annealing Study of Silicon Implanted Aluminum Gallium Nitride," Master's Thesis, Air Force Institute of Technology (AU), Wright-Patterson AFB OH, 2008.

33. J. Fellows, "Electrical Activation Studies of Ion Implanted Gallium Nitride," Ph.D. dissertation, Air Force Institute of Technology (AU), Wright-Patterson AFB OH, 2001.

34. M. Zimpel, M. Oszwaldowski, and J. Goc, *Ada Physica Polonica*, vol. A75, no. 2, pp. 297-300, 1989.

35. G. Johnson, B. Cavenett, T. Kerr, P. Kirby, and C. Wood, "Optical, Halll and cyclotron resonance measurements of GaSb grown by molecular beam epitaxy," *Semiconductor Science Technology*, vol. 3, pp. 1157-1165, 1988.

36. M. Lee, D. Nicholas, K. Singer, and B. Hamilton, "A photoluminescence and Hall-effect study of GaSb grown by molecular-beam epitaxy," *Journal of Applied Physics*, vol. 59, no. 8, pp. 2895-2900, 1986.

37. K. O'Donnell and X. Chen, "Temperature dependence of semiconductor band gaps," *Applied Physics Letters*, vol. 58, no. 25, pp. 2924-2926, 1991.

REPORT DOCUMENTATION PAGE			Form Approved OMB No. 074-0188

The public reporting burden for this collection of information is estimated to average 1 hour per response, including the time for reviewing instructions, searching existing data sources, gathering and maintaining the data needed, and completing and reviewing the collection of information. Send comments regarding this burden estimate or any other aspect of the collection of information, including suggestions for reducing this burden to Department of Defense, Washington Headquarters Services, Directorate for Information Operations and Reports (0704-0188), 1215 Jefferson Davis Highway, Suite 1204, Arlington, VA 22202-4302. Respondents should be aware that notwithstanding any other provision of law, no person shall be subject to an penalty for failing to comply with a collection of information if it does not display a currently valid OMB control number. **PLEASE DO NOT RETURN YOUR FORM TO THE ABOVE ADDRESS.**

1. REPORT DATE (DD-MM-YYYY) 26-03-2009	2. REPORT TYPE Master's Thesis	3. DATES COVERED (From – To) March 2008 – March 2009

4. TITLE AND SUBTITLE Investigation of Electrical and Optical Properties of Bulk III-V Ternary Semiconductors	5a. CONTRACT NUMBER
	5b. GRANT NUMBER
	5c. PROGRAM ELEMENT NUMBER
6. AUTHOR(S) Gomez, Travis C., Captain, USAF	5d. PROJECT NUMBER
	5e. TASK NUMBER
	5f. WORK UNIT NUMBER

7. PERFORMING ORGANIZATION NAMES(S) AND ADDRESS(S) Air Force Institute of Technology Graduate School of Engineering and Management (AFIT/EN) 2950 Hobson Way, Building 640 WPAFB OH 45433-7765	8. PERFORMING ORGANIZATION REPORT NUMBER AFIT/GMS/ENP/09-M01

9. SPONSORING/MONITORING AGENCY NAME(S) AND ADDRESS(ES) Dr. Donald Silversmith AFOSR/NE 875 N. Randolph St., Arlington, VA 22203	10. SPONSOR/MONITOR'S ACRONYM(S)
	11. SPONSOR/MONITOR'S REPORT NUMBER(S)

12. DISTRIBUTION/AVAILABILITY STATEMENT

APPROVED FOR PUBLIC RELEASE; DISTRIBUTION UNLIMITED.

13. SUPPLEMENTARY NOTES

14. ABSTRACT

Bulk grown III-V ternary semiconductors of $In_{0.08}Ga_{0.92}Sb$ and $In_{0.15}Ga_{0.85}As$ were investigated through Hall-effect and photoluminescence measurements to determine carrier concentration, mobility, sheet resistivity, and luminescence spectrum. In the past, epitaxial layers of ternary compounds have been grown on binary compound substrates, and thus very limited lattice matched ternary alloys were available. Recently, bulk grown ternary substrates have been developed, and it has presented a renewed interest in using these substrates to grow high quality ternary compounds for use in many next generation optoelectronic devices. The results of photoluminescence (PL) study for the $In_{0.15}Ga_{0.85}Sb$ sample show the exciton bound to neutral acceptor (A^o,X) transition peak at 0.675 eV along with a donor-shallow acceptor pair transitions at 0.650 eV, and the donor-deep acceptor pair transition peak at 0.628 eV. The Hall-effect measurements show that this sample is an n-type material with carrier concentration of $5.1x10^{17}/cm^3$ and mobility of 660 cm^2/Vs at room temperature. The $In_{0.80}Ga_{0.20}As$ sample is also an n-type material with a carrier concentration of $1.341x10^{16}/cm^3$ and a mobility of 9,670 cm^2/Vs at room temperature. The PL results of this sample shows a broad band to band peak at 0.572 eV. The PL taken at different positions of the sample show different band to band peak positions for the $In_{0.80}Ga_{0.20}As$ sample, indicating a slight inhomogeneity in Ga concentration, while the PL observed from the $In_{0.15}Ga_{0.85}Sb$ sample show position independent. Although the current bulk grown ternary alloy materials may not be as great yet as we hope for a direct use in next generation optoelectronic devices, it will provide suitable substrates for which to grow epitaxial layers.

15. SUBJECT TERMS

Indium Gallium Arsenide, Indium Gallium Antimonide, Electrical Characterization, Optical Characterization, Hall Measurements, Mobility, Conductivity, Carrier Concentration, Photoluminescence, Band Gap, Recombination.

16. SECURITY CLASSIFICATION OF:			17. LIMITATION OF ABSTRACT	18. NUMBER OF PAGES	19a. NAME OF RESPONSIBLE PERSON Dr. Yung Kee Yeo, ENP
a. REPORT	b. ABSTRACT	c. THIS PAGE	UU	65	19b. TELEPHONE NUMBER (Include area code) (937) 255-3636, x5432; email: yung.yeo@afit.edu
U	U	U			

Standard Form 298 (Rev. 8-98)
Prescribed by ANSI Std. Z39-18